Depletion of limiting rDNA structural complexes triggers chromosomal instability and replicative aging of *Saccharomyces cerevisiae*

Ryan D. Fine[1], Nazif Maqani[1], Mingguang Li[1,2], Elizabeth Franck[1], and Jeffrey S. Smith[1,*]

[1]Department of Biochemistry and Molecular Genetics, University of Virginia School of Medicine, Charlottesville, VA 22908. [2]Department of Laboratory Medicine, Jilin Medical University, Jilin, 132013, China

[*]Corresponding Author

Department of Biochemistry and Molecular Genetics

University of Virginia School of Medicine

Pinn Hall, Box 800733

Charlottesville, VA 22908

Phone: 434-243-5864

Fax: 434-924-5069

Email: jss5y@virginia.edu

Keywords: Sir2, cohesin, RENT, monopolin, yeast, replicative lifespan, aging, rDNA

Abstract

Sir2 is a highly conserved NAD^+-dependent histone deacetylase that functions in heterochromatin formation and promotes replicative lifespan (RLS) in the budding yeast, *Saccharomyces cerevisiae*. Within the yeast rDNA locus, Sir2 is required for efficient cohesin recruitment and maintaining stability of the tandem array. In addition to the previously reported depletion of Sir2 in replicatively aged cells, we discovered that subunits of the Sir2 containing complexes, SIR and RENT, were depleted. Several other rDNA structural protein complexes also exhibited age-related depletion, most notably the cohesin complex. We hypothesized that mitotic chromosome instability (CIN) due to cohesin depletion could be a driver of replicative aging. ChIP assays of the residual cohesin (Mcd1-13xMyc) in moderately aged cells showed strong depletion from the rDNA and initial redistribution to the point centromeres, which was then lost in older cells. Despite the shift in cohesin distribution, sister chromatid cohesion was partially attenuated in aged cells and the frequency of chromosome loss was increased. This age-induced CIN was exacerbated in strains lacking Sir2 and its paralog, Hst1, but suppressed in strains that stabilize the rDNA array due to deletion of *FOB1* or through caloric restriction (CR). Furthermore, ectopic expression of *MCD1* from a doxycycline-inducible promoter was sufficient to suppress rDNA instability in aged cells and to extend RLS. Taken together we conclude that age-induced depletion of cohesin and multiple other nucleolar chromatin factors destabilize the rDNA locus, which then results in general CIN and aneuploidy that shortens RLS.

38 ## Introduction

39 Budding yeast replicative lifespan (RLS) was originally described decades ago as the number of
40 times a mother cell divides before losing viability (MORTIMER AND JOHNSTON 1959), and has
41 been an effective model system for the identification and/or characterization of several conserved
42 aging-related genes and pathways, including *SIR2*, AMPK (Snf1), and TOR signaling (WASKO
43 AND KAEBERLEIN 2014). *SIR2* is possibly the most famous yeast gene associated with replicative
44 aging and encodes the founding family member of the NAD^+-dependent histone/protein
45 deacetylases, commonly known as sirtuins (reviewed in (BUCK *et al.* 2004)). The NAD^+
46 dependence of sirtuins provides a direct link between metabolism and cellular processes
47 regulated by these enzymes. In fact, recent evidence points to depletion of cellular NAD^+ pools
48 as a potential mechanism for aging-associated disease, which could be mediated by impairment
49 of sirtuins or other NAD^+ consuming enzymes (GOMES *et al.* 2013). Therefore, understanding
50 how sirtuins are impacted by aging and how they regulate age-altered cellular processes is of
51 intense interest.

52 Eukaryotic genomes generally encode for several sirtuin homologs. The *Saccharomyces*
53 *cerevisiae* genome, for example, encodes *SIR2* and four additional Homologs of Sir Two (*HST1-*
54 *HST4*) (BRACHMANN *et al.* 1995; DERBYSHIRE *et al.* 1996). Sir2 and its fellow Silent Information
55 Regulator proteins, Sir1, Sir3, and Sir4 were originally shown to establish and maintain silencing
56 of the silent mating loci, *HML* and *HMR* (RINE AND HERSKOWITZ 1987). These proteins form the
57 so-called SIR complex that is recruited to and then spreads across the *HM* loci and telomeres to
58 form hypoacetylated heterochromatin-like domains (reviewed in (GARTENBERG AND SMITH
59 2016)). Sir2 is required for replicative longevity and its abundance is significantly reduced in
60 replicatively aged yeast cells (DANG *et al.* 2009), presenting a possible mechanism for the

61 decline of Sir2-dependent processes during aging. including gene silencing. Indeed, the depletion
62 of Sir2 in aged cells causes hyperacetylated H4K16 and silencing defects at subtelomeric loci
63 (DANG *et al.* 2009). It has been reported that aged cells become sterile (mating-incompetent) due
64 to loss of silencing at *HML* and *HMR* (SMEAL *et al.* 1996), which results in co-expression of the
65 normally repressed α1/α2 and a1/a2 transcription factor genes encoded at these loci. In theory,
66 this should induce a diploid-like or "pseudodiploid" gene expression pattern and sterility, as is
67 observed for a silencing defective *sir2*Δ mutant (RINE AND HERSKOWITZ 1987). However, more
68 recent experiments point toward a silencing-independent mechanism of sterility, whereby
69 aggregation of the Whi3 protein in aged cells makes them insensitive to pheromones (SCHLISSEL
70 *et al.* 2017).

71 Alternative models for Sir2 control of RLS have focused on the rDNA tandem array
72 where Sir2 is important for cohesin recruitment (KOBAYASHI *et al.* 2004; GANLEY AND
73 KOBAYASHI 2014). Cohesin association with the rDNA also requires Tof2 and the Lrs4/Csm1
74 (cohibin) complex (HUANG *et al.* 2006). Sir2 silences RNA polymerase II-dependent
75 transcription at the rDNA locus via a nucleolar HDAC complex called RENT (BRYK *et al.* 1997;
76 SMITH AND BOEKE 1997), consisting of Sir2, Net1, and Cdc14 subunits (SHOU *et al.* 1999;
77 STRAIGHT *et al.* 1999). Specifically, RENT represses transcription of endogenous non-coding
78 RNAs from the intergenic spacer (IGS) regions (LI *et al.* 2006). Derepression of the bidirectional
79 promoter (E-pro) within IGS1 in *sir2*Δ cells displaces cohesin from the rDNA, thus destabilizing
80 the array by making it more susceptible to unequal sister chromatid exchange (KOBAYASHI AND
81 GANLEY 2005). Mild Sir2 overexpression, on the other hand, enhances silencing, suppresses
82 recombination between repeats, and extends RLS (SMITH *et al.* 1998; KAEBERLEIN *et al.* 1999).

83 Extrachromosomal rDNA circles (ERCs) derived from these unequal recombination
84 events specifically accumulate to high levels in old mother cells (SINCLAIR AND GUARENTE
85 1997), where they can interfere with G1 cyclin expression (NEUROHR *et al.* 2018). Such an ERC-
86 centric model is supported by RLS extension of *fob1*Δ strains (DEFOSSEZ *et al.* 1999). Fob1
87 binds to the rDNA at IGS1 to block DNA replication forks from colliding with elongating RNA
88 polymerase I molecules (KOBAYASHI AND HORIUCHI 1996). The blocked forks can collapse,
89 resulting in double-stranded DNA breaks that trigger unequal sister chromatid exchange
90 (TAKEUCHI *et al.* 2003). The frequency of rDNA recombination and ERC production is reduced
91 in a *fob1*Δ mutant due to loss of the fork block, thus extending RLS (DEFOSSEZ *et al.* 1999).
92 More recently, this rDNA-centric model of aging has been extended to include general rDNA
93 instability having negative effects on genome integrity, including ERC accumulation, and is also
94 considered a critical contributor to aging (GANLEY AND KOBAYASHI 2014).
95 In addition to promoting cohesin recruitment to the rDNA, Sir2 is also required for
96 establishing sister chromatid cohesion (SCC) at *HML* and *HMR* (CHANG *et al.* 2005; WU *et al.*
97 2011). Moreover, we previously observed significant overlap between Sir2 and cohesin at
98 additional binding sites throughout the genome (LI *et al.* 2013). Outside heterochromatin, the
99 cohesin loading complex (Scc2/Scc4) deposits cohesin (Mcd1, Irr1, Smc1, Smc3) onto
100 centromeres and other cohesion associated regions (CARs) (CIOSK *et al.* 2000; KOGUT *et al.*
101 2009), in order to maintain SCC until anaphase, when Mcd1 is cleaved by separase to facilitate
102 sister chromatid separation (reviewed in (MARSTON 2014)). Cohesin defects therefore result in
103 chromosome instability (CIN) due to improper chromosome segregation (reviewed in (WOOD *et*
104 *al.* 2010)). A previous study found that cells deleted for *SIR2* have a CIN phenotype related to
105 hyperacetylation of H4K16 (CHOY *et al.* 2011), though the functional relationship to cohesin was

106 not considered. Given the natural depletion of Sir2 from replicatively aging yeast cells (DANG *et*
107 *al.* 2009), we hypothesized the frequency of CIN should increase with age. Here, we establish
108 that CIN is indeed more frequent in aged cells and is associated with SCC defects. We go on to
109 show that like Sir2, cohesin subunits are depleted from aged mother cells, providing a likely
110 reason for problems with SCC. Interestingly, despite the overall reduction in cohesin protein
111 levels, the chromosomal distribution of cohesin enrichment was not uniform. In moderately aged
112 mother cells, enrichment at the rDNA was drastically reduced, while binding at centromeres was
113 not, suggesting a mechanism by which SCC is preferentially maintained at centromeres to ensure
114 cell viability. However, this comes at the expense of chronic rDNA instability that is exacerbated
115 by additional age-induced reductions in the RENT and cohibin/monopolin complexes. The
116 defects in rDNA stability can be suppressed by overexpressing the Mcd1 subunit of cohesion,
117 which also extends RLS, thus making cohesin a dose dependent longevity factor. Lastly, the age
118 associated CIN phenotype is suppressed by deleting *FOB1* or by CR growth conditions,
119 suggesting a model whereby rDNA instability on chromosome XII caused by RENT, cohibin,
120 and cohesin depletion drives the mitotic segregation defects of other chromosomes during
121 replicative aging.
122

123 ## Methods

124 **Yeast strains, plasmids, and media**

125 Yeast strains were grown at 30°C in Yeast Peptone Dextrose (YPD) or Synthetic
126 Complete (SC) medium for strains bearing plasmids (MATECIC *et al.* 2010). *SIR2, HST1*, or
127 *FOB1* open reading frames were disrupted with one-step PCR-mediated gene replacement using
128 *kanMX4*, *natMX4*, or *hphMX4* drug resistance markers, respectively. The *HMR* deletion by

129 replacement with *hphMX4* spans sacCer3 genome chrIII coordinates 293170-294330. All C-
130 terminally 13xMyc (EQKLISEEDL) tagged proteins were targeted at endogenous loci in the
131 Mother Enrichment Program (MEP) strains UCC5181 and UCC5179 (LINDSTROM AND
132 GOTTSCHLING 2009), followed by mating to generate homozygous diploids. All deletions and
133 fusions were confirmed by colony PCR, western blotting, or both. pRF4 was constructed by PCR
134 amplifying the *MCD1* open reading frame from ML1 genomic DNA and ligating into *Pst*I and
135 *Not*I sites of pCM252 (BELLI *et al.* 1998), a tetracycline inducible overexpression vector
136 (Euroscarf). pRF10 and pRF11 were constructed by removing the expression cassette by *Pvu*II
137 blunt end digestion of pCM252 and pRF4, respectively, and ligating it between the *Pvu*II sites of
138 pRS405 bearing *LEU2*, thus replacing the *TRP1* marker with *LEU2*. pRF10 and 11 were then
139 digested with *EcoRV* and integrated into the genome at *leu2Δ1*. pSB760 and pSB766 are
140 integrating and *2μ LEU2* vectors, respectively, bearing a single copy of *SIR2* (BUCK *et al.* 2002).
141 All strains used in this work are listed in Table S1 and all primers are listed in Table S2.
142
143 **Isolation of aged yeast cells**
144 Aged yeast cell enrichment was based on the MEP strain background (LINDSTROM AND
145 GOTTSCHLING 2009; LINDSTROM *et al.* 2011). For all assays, 1 μL of stationary phase culture
146 was inoculated into 100 mL of YPD medium and then grown into log phase. Approximately
147 $1x10^8$ cells were harvested, and centrifuged cell pellets washed 3 times with 1x phosphate
148 buffered saline (PBS). Cells were then resuspended in 1 mL PBS and mixed with 5 mg of Sulfo-
149 NHS-LC-Biotin (Pierce) per $1x10^8$ cells for 30 min at room temperature. After biotin labeling,
150 $5x10^7$ cells were added to 1.5 L YPD cultures containing 1 μM estradiol, and 100 μg/mL
151 ampicillin to prevent bacterial contamination. These cultures were allowed to grow for 24 hr to

152 36 hr before processing in an assay specific manner (see below). For non-MEP strain
153 backgrounds, estradiol was not added to the cultures.
154
155 **Western blotting**
156 Two 1.5 L cultures were used for each western blot experiment, corresponding to
157 approximately $2x10^7$ total aged cells after purification for each biological replicate. Cells were
158 pelleted using a Sorvall RC-5B Plus centrifuge with an SLA-3000 rotor at 2000 rpm, then
159 resuspended at a density of $6x10^8$ cells/mL in RNAlater (Ambion) for 45 min in two separate
160 conical tubes. Following fixation, cells were pelleted and resuspended in 45 mL of cold PBS, 2
161 mM EDTA in 50 mL conical tubes. The mixture was incubated at 4°C for 30 min with 800 µL of
162 Streptavidin MicroBeads (Miltenyi Biotec), which were then purified through an autoMACS Pro
163 Cell Separator using the posseld2 program (UVA Flow Cytometry Core Facility). A 20 µL
164 aliquot of each output was used for bud scar counting using calcofluor white staining, before
165 combining the isolated samples into a single microfuge tube. Samples were frozen at -80°C
166 before protein extraction. Thawed cells were vortexed twice for 1 min in 20% TCA
167 (trichloroacetic acid) with ~100 µL of acid washed glass beads with a brief cooling period in
168 between vortexing. Beads were allowed to settle before transferring the supernatant to a fresh
169 microfuge tube. A 250 µL wash of 5% TCA was applied twice to the beads and pooled with the
170 initial lysis sample. Proteins were precipitated at 10,000 rpm in a microfuge for 5 min at 4°C.
171 Pellets were then resuspended in 50 µL of 1x SDS sample buffer (50 mM Tris-HCl pH 6.8, 2%
172 SDS, 10% Glycerol, 3.6 M 2-mercaptoethanol) and neutralized with 30 µL of 1M Tris-HCl, pH
173 8.0. Samples were run on a 9% (w/v) SDS-polyacrylamide gel and transferred to an Immobilon-
174 P membrane (Millipore). Membranes were incubated for 1 hour at room temperature in 1xTBST

175 + 5% non-fat milk with primary antibodies (1:2000 α-Myc 9E10, 1:5000; α-Vma2 (Life
176 Technologies); 1:5000 α-Sir2 (Santa Cruz Biotechnology); 1:1000 α-Sir4 (Santa Cruz
177 Biotechnology); 1:1000 α-Sir3 (Santa Cruz Biotechnology). HRP-conjugated secondary
178 antibodies (Promega) were diluted 1:5000, and detected using chemiluminescence with HyGLO
179 (Denville Scientific). Quantitation was performed with ImageJ by using the rectangle tool to
180 outline protein bands and an equivalent sized box for background. After subtraction of
181 background, the signal of the aged cell band was divided by the signal of the Vma2 loading
182 control, and finally normalized to the quantity of the Vma2 normalized young cell band which
183 was arbitrarily set at 1.0.
184
185 **ChIP Assays with aged and young cell populations**
186 Two 1.5 L cultures were used for each biological replicate. After centrifugation, cells
187 were washed with 1xPBS then resuspended with 45 mL of PBS and incubated with 800 µL of
188 streptavidin microbeads, followed by sorting with the autoMACS Pro Cell Separator. Sorted
189 cells were immediately crosslinked with 1% formaldehyde for 20 min at room temperature, then
190 transferred to screw cap microcentrifuge tubes and the pellets flash frozen in liquid nitrogen.
191 Cells were thawed and lysed in 600 µL FA140 Lysis buffer (50 mM HEPES, 140 mM NaCl, 1%
192 Triton X-100, 1 mM EDTA, 0.1% SDS, 0.1 mM PMSF, 1x protease inhibitor cocktail; Sigma)
193 by shaking with acid-washed glass beads in a Mini-Bead beater (Biospec Products). Cell lysates
194 were recovered and sonicated for 30 cycles of 30 sec "on" and 30 sec "off" in a Diagenode
195 Bioruptor followed by centrifugation at 16,000 x g. A 1/10th supernatant volume input was taken
196 for each sample and crosslinking reversed by incubating overnight at 65°C in 150 µL elution
197 buffer (TE, 1% SDS). The remaining supernatant was used for immunoprecipitation overnight at

198 4°C with 5 µg of primary antibody and 30 µL of protein G magnetic beads (Pierce), followed by
199 washing 1x with FA-140 buffer, 2x with FA-500 buffer (FA-140 with 500 mM NaCl), and 2x
200 with LiCl solution (10 mM Tris-HCl, pH 8.0, 250 mM LiCl, 0.5% NP-40, 0.5% SDS, 1 mM
201 EDTA). DNA was eluted twice with 75 µL of elution buffer in a 65°C water bath for 15 min.
202 The eluates were combined and crosslinking reversed. Input and ChIP DNA samples were
203 purified by an Invitrogen PureLink™ PCR purification kit. Finally, ChIP DNA was quantified by
204 real-time PCR and normalized to the input DNA signal. Young cells were collected flow-through
205 from the autoMACS cell sorter and then processed as described for the aged cells.
206
207 **Sister chromatid cohesion assay**
208 From 50 mL log phase SC cultures of strains 3349-1B, 3312-7A, 3460-2A, RF258,
209 RF278, and RF290, $5x10^7$ cells were washed and biotinylated as described in the Isolation of
210 aged yeast cells section. This population was transferred into a 1.5 L SC culture and allowed to
211 grow for 14 hr. The original biotinylated cells were then purified by incubation with 300 µL of
212 streptavidin micro beads followed by gravity filtration through a Miltenyi LS column. The
213 column was washed twice with 5 ml of PBS and then processed as described below for young
214 cells.
215 From the original log phase culture, $5x10^7$ cells were transferred to a fresh 50 mL SC
216 culture and arrested in mitosis with 10 µg/mL nocodazole for 1.5 hr. For the *mcd1-1* strain 3312-
217 7A, cells were also shifted to 37°C at this time. For bud scar staining, 5 mg of calcofluor white
218 was dissolved in 1 mL of PBS and any remaining aggregate removed by centrifugation. The 1
219 mL of soluble calcofluor was then added to the 50 mL SC culture. Non-arrested cells were
220 directly stained with calcofluor. Cells were then pelleted and washed in PBS. Following staining,

221 200 µL of 4% paraformaldehyde was added directly to the cell pellet and allowed to crosslink for
222 15 min at room temperature. The cell pellet was washed once with PBS and resuspended in
223 ~100-200 µL of 0.1 $MKPO_4$/1 M sorbitol, pH 6.5. Images were captured with a Zeiss Axio
224 Observer z1 widefield microscope using a 64x oil objective lens.
225
226 **Replicative lifespan assays**
227 Lifespan assays were carried out as previously described (STEFFEN *et al.* 2009). Briefly,
228 small aliquots of log phase cultures were dripped in a straight line onto solid agar YPD with 2%
229 glucose. From the initial populations, a minimum of 32 virgin daughter cells were picked for
230 lifespan assays with daughter cells being selectively pulled away from mother cells using a
231 fiberoptic dissection needle and on a Nikon Eclipse 400 microscope. All virgin daughters were
232 required to bud at least one time to be included in the experiment and dissection was carried out
233 over the course of several days with temporary incubation at 4°C in between dissection periods
234 to stop division. Cells were considered dead when they stopped dividing for a minimum of 2
235 generation times (180 min). For p-values indicated in the text, a Wilcoxon rank-sum test was
236 conducted for respective lifespan assays using the basic wilcox.test function in R.
237
238 **Mini-chromosome loss (sectoring) assay**
239 The colony sectoring assay was performed on SC plates with adenine limited to 80 µM.
240 Frequency of mini-chromosome loss represents the number of ½ red/white sectored colonies
241 divided by the sum of sectored and white colonies. Cells were plated to an approximate density
242 of 500 cells/plate based on counts from a Brightline hemocytometer. Any plates bearing greater
243 than 1000 cells were discarded. Three biological replicates of each strain were performed, with at

244 least 10 plates counted per replicate. For aged cell populations, ~5x10^6 biotinylated cells were
245 aged in 1.5 L of YPD for 24 hr. Cells were incubated with 300 µL of streptavidin magnetic beads
246 (New England Biolabs) and manually washed 4 times with PBS on a magnetic stand, then plated
247 onto the limiting adenine SC plates such that ~500 colonies appeared. Bud scars were not
248 counted because the size of the beads prohibited visualization.
249
250 **RT-qPCR measurement of *MCD1* overexpression**
251 Doxycycline was added to log phase cultures at a concentration of 2 µg/mL for 4 hr in
252 order to induce expression of *MCD1*. Total RNA was extracted using a standard acid phenol
253 extraction protocol (AUSUBEL *et al.* 2000). cDNA was created from 1 µg of RNA using a Verso
254 cDNA synthesis kit (Thermo Fisher). *MCD1* expression levels were quantified on an Applied
255 Biosystems StepOne real time PCR machine with primers JS2844 and JS2949, and normalized to
256 actin transcript levels (primers JS1146 and JS1147).
257
258 **Hi-C library construction**
259 Log-phase cultures were cross-linked with 3% formaldehyde for 20 min and quenched
260 with a 2x volume of 2.5M glycine. Cell pellets were washed with dH_2O and stored at -80°C.
261 Thawed cells were resuspended in 5 ml of 1X NEB2 restriction enzyme buffer (New England
262 Biolabs) and poured into a pre-chilled mortar containing liquid N_2. Nitrogen grinding was
263 performed twice as previously described (BELTON AND DEKKER 2015), and the lysates were then
264 diluted to an OD_{600} of 12 in 1x NEB2 buffer. 500 µl of cell lysate was used for each Hi-C library
265 as follows. Lysates were solubilized by the addition of 50 µl 1% SDS and incubation at 65°C for
266 10 min. 55 µl of 10% Triton X-100 was added to quench the SDS, followed by 10 µl of 10X

267 NEB2 buffer and 15 µl of *Hin*dIII (New England Biolabs, 20 U/µl) to digest at 37°C for 2 hr. An
268 additional 10 µl of *Hin*dIII was added for digestion overnight. The remainder of the protocol was
269 based on previously published work with minor exceptions (BURTON *et al.* 2014). In short, ends
270 were filled in with dNTPs and biotinylated dCTP at 0.4 mM concentration using Klenow Exo-
271 (NEB) for 1 hr at 37°C. After a brief heat inactivation, blunt ends were ligated together in 3 mL
272 reaction volumes with T4 DNA-ligase for 6 hr at 16°C with a minimum DNA concentration of
273 0.5 ng/µL. Following ligation, cross-links were reversed at 70°C O/N and DNA was purified by
274 phenol/chloroform extraction and ethanol precipitation. Unligated-biotinylated ends were
275 removed using T4 DNA Polymerase (NEB). DNA was purified one final time with two
276 Zymogen DNA Clean and Concentrate-5 Kit columns per ligation reaction and eluted with 65
277 µL TE (130 µL total). Chromatin was quantitated with a Qubit fluorometer and then sheared
278 using a Diagenode Bioruptor. Hi-C sequencing libraries were prepared with reagents from an
279 Illumina Nextera Mate Pair Kit (FC-132-1001) using the standard Illumina protocol of End
280 Repair, A-tailing, Adapter Ligation, and 12 cycles of PCR. PCR products were size selected and
281 purified with AMPure XP beads before sequencing with an Illumina Miseq or Hiseq.
282
283 **Hi-C data analysis**
284 Iteratively corrected heatmaps appearing in this manuscript were produced using python
285 scripts from the Mirny lab hiclib library, publicly available at:
286 http://mirnylab.bitbucket.org/hiclib/index.html. Briefly, reads were mapped using the iterative
287 mapping program and then run through the fragment filtering program using the default
288 parameters. Raw heat maps were further filtered to remove diagonal reads and iteratively
289 corrected. Finally, the iteratively corrected heatmaps were normalized for read count differences

290 to make them comparable. The *cdc15-2* sample data was pulled from the SRA database at
291 SRP094582 (LAZAR-STEFANITA *et al.* 2017), and our data is available from GEO at GSE117037.
292
293 **Data availability**
294 Strains and plasmids are available upon request. Supplemental Tables S1 and S2, containing lists
295 of all strains and oligodeoxynucleotides used in the study, are included in the Supplemental
296 Information file. Supplemental Figures S1 through S7 are also included in the same file.
297

298 ## Results

299 **Sir2 binding partners are depleted in aged yeast cells**

300 Sir2 is a dosage dependent longevity factor, such that strains provided one extra *SIR2*
301 gene copy have an extended RLS (KAEBERLEIN *et al.* 1999). Mother cells experience a
302 progressive reduction of Sir2 protein during normal replicative aging that presumably contributes
303 to the aging process (DANG *et al.* 2009). Sir2 does not function in isolation, so we hypothesized
304 that protein levels of key Sir2-interacting partners could also be depleted with age. To isolate
305 sufficient quantities of aged cells for western blot assays we turned to Mother Enrichment
306 Program (MEP) strains developed by the Gottschling lab (LINDSTROM AND GOTTSCHLING 2009).
307 The aged cell purification procedure was validated by increased average bud scar counts with
308 calcofluor white and the expected reduction of Sir2 protein (Figure 1A). The vacuolar protein
309 Vma2, used as a loading control for these western blots, does not deplete with age (LINDSTROM
310 *et al.* 2011). Since Sir2 is the catalytic subunit of both SIR and RENT (Figure 1B), it was
311 important to know which complexes were impacted by age. As shown in Figure 1C and D, Sir4
312 was strongly depleted in aged cells while Sir3 was actually enriched. Sir3 enrichment in aged

313 cells was also observed in an earlier proteomics screen (JANSSENS *et al.* 2015). Such a stark
314 difference was considered relevant because Sir2 and Sir4 interact as a heterodimer that associates
315 with the acetylated H4 N-terminal tail (MOAZED *et al.* 1997), while Sir3 is subsequently
316 recruited following H4K16 deacetylation to complete SIR holocomplex formation on
317 heterochromatin (OPPIKOFER *et al.* 2011). Myc-tagged Net1 (RENT complex) was also strongly
318 depleted from aged cells (Figure 1E), indicating that Sir2/Sir4 and the nucleolar RENT complex
319 are both depleted during aging. It should be noted that the Sir2 paralog, Hst1, which has the
320 capacity to compensate for loss of Sir2 (HICKMAN AND RUSCHE 2007; LI *et al.*), was also
321 partially depleted from aged cells (Figure 1F). Detailed bud scar and protein quantitations from
322 triplicate biological samples are reported in Table S3.
323
324 **Chromosome instability (CIN) increases during replicative aging**
325 Considering the observed depletion of multiple heterochromatin factors in aged yeast
326 cells, as well as the CIN phenotype of a *sir2*Δ mutant (CHOY *et al.* 2011), we next tested whether
327 aged cells had a CIN phenotype that was exacerbated by complete loss of *SIR2* and/or *HST1*.
328 Strains utilized for this experiment have an artificial chromosome III bearing a suppressor tRNA
329 gene, *SUP11* (SPENCER *et al.* 1990). Loss of the chromosome prevents suppression of an ochre
330 stop codon in *ade2-101*, resulting in the classic *ade2* red colony phenotype. The frequency of
331 nondisjunction events was measured by counting half-sectored red/white colonies from young
332 and aged cell populations (Figure 1G). Sectoring was elevated in young populations of *sir2*Δ
333 and *hst1*Δ mutants, and additively increased in a *sir2*Δ*hst1*Δ double mutant (Figure 1H, black
334 bars, left side of panel). Interestingly, sectoring was significantly higher for aged populations of
335 each strain (Figure 1H, gray bars, left side of panel), suggesting additional age-associated factors

336 were involved. We next tested whether the *sir2*Δ effect on sectoring was related to a
337 pseudodiploid phenotype caused by derepression of the *HM* loci. This reporter strain background
338 was *MAT*α, so we deleted *HMR* (chrIII 293170-294330) to eliminate the a1/a2 transcription
339 factors. Reversal of the pseudodiploid phenotype was confirmed by restoration of mating to the
340 *sir2*Δ *hmr*Δ strains (data not shown). Importantly, this manipulation significantly suppressed
341 sectoring of the young *sir2*Δ and *sir2*Δ *hst1*Δ mutants, but not the *hst1*Δ mutant (Figure 1H,
342 middle of panel), indicating there was indeed a *sir2*Δ-induced pseudodiploid effect that
343 contributed to mini-chromosome loss (Figure 1H, black bars, middle of panel). However, aging
344 still increased sectoring in each strain even when *HMR* was deleted (Figure 1H, gray bars,
345 middle of panel), suggesting that the aging-associated CIN factor was unrelated to mating type
346 control.

347 Because of the observed Net1 depletion (Figure 1E), we hypothesized that age-induced
348 mini-chromosome loss could be related to rDNA instability caused by loss of the RENT
349 complex. To address this idea, *FOB1* was deleted from WT, *sir2*Δ, *hst1*Δ, and *sir2*Δ *hst1*Δ
350 reporter strains to stabilize the rDNA, followed by retesting the sectoring phenotypes. As shown
351 in Figure 1H (right side of panel), frequency of sectoring observed for each aged *fob1*Δ strain
352 was generally similar to that observed with young $FOB1^+$ versions of the strains (Figure 1H,
353 black bars, left side of panel), suggesting that destabilization of the rDNA during aging does
354 contribute to the instability of other chromosomes. The *hmr*Δ and *fob1*Δ mutations were
355 potentially suppressing chromosome loss through independent mechanisms, thus begging the
356 question of whether combining them would fully suppress CIN in a *sir2*Δ *hst1*Δ *hmr*Δ *fob1*Δ
357 quadruple mutant. Remarkably, aged cells from this mutant combination lost the mini

358 chromosome marker at a very low rate comparable to young WT cells, with no statistical
359 difference (Figure 1H, 1-way ANOVA).
360
361 **Cohesin levels are depleted in aged yeast cells**
362 The above results raised the question of what factor(s) related to rDNA stability,
363 chromosome segregation, and Sir2, was becoming defective in aged cells. Cohesin perfectly fit
364 this profile and was earlier shown in mammalian oocytes to become depleted with age (reviewed
365 in (JESSBERGER 2012)). To test whether cohesin was another Sir2-linked factor depleted during
366 yeast aging, we C-terminally myc-tagged the Mcd1 or Smc1 subunits (Figure 2A) in the MEP
367 strain background. Western blotting demonstrated that both subunits were significantly depleted
368 from aged cells (Figure 2B), implying depletion of the whole cohesin complex. We also
369 observed depletion of the cohibin/monopolin subunit Lrs4 (Figure S2), which can function as a
370 cohesin clamp at the rDNA (HUANG *et al.* 2006). Furthermore, a Myc-tagged Scc2 subunit of the
371 Scc2/Scc4 cohesin loading complex was age-depleted (Figure 2C), though not as severely as the
372 cohesin complex, predicting that the remaining cohesin complex could still be loaded onto
373 chromatin in aged cells. ChIP assays for Mcd1-myc in MEP cells aged for 24 hr demonstrated
374 strong depletion from the rDNA intergenic spacer (IGS1) (Figure 2D), but was surprisingly
375 enriched at the centromeres of chromosomes XI and III. This effect did not appear to
376 significantly extend into the pericentric region of chromosome III (Figure 2E). In order to rule
377 out primer specificity or chromosome size effects, we tested three centromeres from other
378 chromosomes and observed the same trend for each of them (Figure 2F). To confirm the
379 enrichment was centromere specific, we tested two additional sites on chromosome IV that were
380 15kb and 200kb away from the centromere, and observed no increase in the aged samples

381 compared to young (Figure 2G). To test if the enrichment of Mcd1-myc at centromeres in aged
382 cells was specific to cohesin, and not a ChIP artifact, we next tested the distribution of Sir4-myc,
383 which was also depleted from aged cells (Figure 1C). In this case, Sir4-myc was depleted from
384 *TELXV* in aged cells (one of its normal targets) without any apparent redistribution to
385 centromeres (*CEN4*) or the rDNA (Figure 2H), indicating that not all age-depleted proteins
386 become enriched at centromeres. Based on these results, we hypothesized that as cohesin starts
387 depleting during replicative aging, its association with the rDNA is severely affected while a
388 significant portion of the remaining complex is retained and potentially redistributed to
389 centromeres. This is consistent with an earlier finding that cohesin preferentially associates with
390 pericentromeric regions instead of chromosome arms when Mcd1 expression is artificially
391 reduced below 30% of normal (HEIDINGER-PAULI *et al.* 2010). We next asked if the centromere
392 enrichment would be lost in an older cell population by extending growth of the MEP culture
393 time course to 36 hr. As shown in Figure 2I, the Mcd1-Myc association with *CEN4* and *CEN14*
394 returned to the original levels observed in young cells, while remaining depleted at the rDNA
395 array (Fig 2J). It is important to note that in a recent report (PAL *et al.* 2018), cohesin enrichment
396 at centromeres was actually reduced in very old yeast cells (>25 generations). Combined with
397 our findings, a model emerges whereby cohesin enrichment at centromeres is initially enhanced
398 during aging, but then catastrophically lost as cells approach the end of their lifespan.
399
400 **Sister chromatid cohesion is compromised in aged yeast cells**
401 Previous work found that SCC was surprisingly normal despite the forced reduction
402 (<30%) of Mcd1 protein levels (HEIDINGER-PAULI *et al.* 2010), leading us to ask whether
403 cohesion would be maintained in our moderately aged yeast cells that were also depleted for

404 cohesin, yet still showed enrichment at centromeres. To this end, we utilized strains with a LacO
405 array located approximately 10 kb away from centromere IV (*CEN4*) as a proxy for centromeric
406 cohesion, or at the *LYS4* locus on chromosome IV, located approximately 400 kb away from the
407 centromere, as a proxy for arm cohesion (UNAL *et al.* 2008; GUACCI AND KOSHLAND 2012).
408 Differential positioning of the array had no significant impact on RLS (Figure S3). SCC was
409 monitored by LacI-GFP appearing either as one dot in the case of cohesion maintenance or two
410 dots in the case of cohesion loss. Using an *mcd1-1* temperature sensitive mutant as a positive
411 control (GUACCI *et al.* 1997), we observed a large increase in two dots when cells were
412 synchronized in mitosis with nocodazole and shifted to 37°C (Figure 3A and B). WT cells for the
413 equivalent reporter strain were next biotinylated and aged for 24 hours, followed by purification
414 with magnetic streptavidin beads and arrest with nocodazole. Analyzing cells with >7 bud scars,
415 which is older than the average bud scar count of our western blot experiments, revealed a mild
416 loss of cohesion (Figure 3C and D). A similar analysis was then performed without the use of
417 nocodazole to rule out any side-effects related to triggering the mitotic spindle checkpoint. To
418 avoid misinterpreting anaphase events as lost SCC, we C-terminally tagged the spindle pole body
419 subunit Spc42 with dsRED, and only counted GFP dots from large-budded cells where the
420 spindle pole bodies had not separated between the mother and daughter cell. With this analysis,
421 the fold-change of SCC defect between young and aged cells was more pronounced (Figure 3E
422 and F), but the absolute frequency of loss was still much weaker than observed with the *mcd1-1*
423 mutant, which was not surprising given that mean lifespan of this strain background is ~16
424 generations (Figure S3). In very old cells (>25 bud scars) of a different strain background, an
425 independent study observed SCC loss on chromosome XII at a frequency that approached 50%

426 (PAL *et al.* 2018) suggesting that CIN may become most severe in the oldest cells where cohesin
427 is not only depleted from the rDNA, but also from centromeres.
428
429 **RLS is modulated by Mcd1 expression levels**
430 Since Sir2 and cohesin are both naturally depleted from replicatively aging yeast cells
431 (Figures 1A and 2B), and mild Sir2 overexpression extends RLS (KAEBERLEIN *et al.* 1999), we
432 hypothesized that manipulating cohesin expression levels would also impact CIN and RLS in a
433 dose-dependent manner. We initially attempted to overexpress the Mcd1 subunit from a
434 galactose inducible *GAL1* promoter and then measure mini-chromosome loss frequency by
435 counting ½ sectored colonies. However, simply growing the reporter strain in galactose-
436 containing media, even with an empty expression cassette, resulted in severe mini-chromosome
437 loss compared to glucose-containing media (Figure 4A and B). This effect was specific to
438 galactose, as growth with another non-preferred carbon source (raffinose) had no effect on
439 sectoring (Figure 4A and B). Though not useful for assaying the effects of *MCD1*
440 overexpression, it was still possible that the unexpectedly high CIN phenotype would correlate
441 with reduced RLS. We therefore measured RLS with the mini-chromosome reporter strain on
442 YEP plates with 2% glucose, galactose, or raffinose. As shown in Figure 4C, galactose strongly
443 decreased the mean RLS by ~50% compared to glucose (9.2 vs. 18.9 divisions, $p<1.0x10^{-15}$),
444 while raffinose only had a marginal effect (15.5 divisions, $p<0.01$). To confirm the galactose
445 effect on RLS was not specific to the mini-chromosome strain, lifespan assays were repeated
446 with the commonly used strains BY4741 (*MAT*a) and BY4742 (*MAT*α). Again, a significant
447 decrease in mean lifespan was observed for BY4741 (17.7 divisions) and BY4742 (18.9
448 divisions) on galactose as compared to glucose (24.3 and 24.2 divisions, respectively) (Figure

449 S4, $p<0.001$), suggesting that galactose triggers a high rate of CIN through an unknown
450 mechanism that also shortens RLS.
451 To circumvent the use of galactose for *MCD1* overexpression we turned to an inducible
452 "Tet-On" promoter that is activated by doxycycline (BELLI *et al.* 1998). Strains harboring this
453 integrated cassette transcriptionally overexpressed *MCD1* approximately 2- to 7-fold compared
454 to the empty vector control (Figure S5A and B). In the mini-chromosome reporter strain, *MCD1*
455 overexpression significantly reduced the frequency of ½ sectored colonies in both young and
456 aged populations (Figure 4D), in agreement with *MCD1* being isolated as a high copy suppressor
457 of CIN using a different reporter system (ZHU *et al.* 2015). Next, *MCD1* was overexpressed in a
458 strain containing an ochre stop codon in the *MCD1* open-reading frame (*mcd1L12STOP*) that
459 reduces Mcd1 protein to ~30% of normal (HEIDINGER-PAULI *et al.* 2010). With an empty
460 pCM252 control *CEN* vector, *mcd1L12STOP* exhibited a 40% reduction in mean RLS (9.9
461 divisions) compared to an isogenic WT control (16.5 divisions), indicating that Mcd1 depletion
462 shortens RLS (Figure 4E, $p<0.001$). Overexpressing *MCD1* almost fully restored longevity to the
463 mutant (14.7 divisions) and, remarkably, also extended RLS of the control WT strain to 19.6
464 divisions ($p<1.0\times10^{-7}$), which was primarily due to improved survival during the first ~15
465 divisions and then followed by a steeper decline in viability (Figure 4E). This biphasic pattern
466 was highly reproducible and suggested that the *CEN MCD1* OE plasmid was being lost around
467 mid-life due to increased chromosome loss, as previously seen in aged cells of our CIN assay
468 (Figure 1H). To account for this potential variable, we also integrated the empty and *MCD1* OE
469 vectors into a different FY834 strain background related to the long lived BY4741/42
470 background (WINSTON *et al.* 1995; BRACHMANN *et al.* 1998). Not only did *MCD1* OE extend the
471 mean RLS (28.0 divisions) in this background compared to the control (21.0 divisions), but the

472 maximum number of divisions was also increased by 25% (Figure S6, $p<1.0x10^{-7}$). We therefore
473 conclude that similar to Sir2, Mcd1 is a strong dose-dependent longevity factor.
474 Sir2 functions upstream of cohesin for RLS (KOBAYASHI *et al.* 2004; KOBAYASHI AND
475 GANLEY 2005), and for SCC at *HMR* (WU *et al.* 2011), implying that Sir2 is upstream of cohesin
476 loading and function. However, this relationship could potentially be more complex since both
477 factors are depleted with age. To explore this further, we next tested if *SIR2* overexpression
478 could rescue the short RLS of an Mcd1-depleted *mcd1L12STOP* strain by integrating a second
479 copy of *SIR2* (2x*SIR2*) at the *LEU2* locus. As shown in Figure 4F, 2x*SIR2* partially rescued mean
480 RLS of the *mcd1L12STOP* strain (14.1 versus 9.9 divisions, $p<1.0x10^{\wedge-4}$), and also increased
481 maximum RLS of the WT strain. Reciprocally, we asked if *MCD1* overexpression would
482 suppress the short RLS of a *sir2*Δ or *sir2*Δ *hst1*Δ mutant. The double mutant was included to rule
483 out any redundancy between the two sirtuins. Mean RLS was clearly not increased by *MCD1*
484 overexpression as compared to empty vector for either the single (10.7 versus 10.2) or double
485 mutant (10.1 versus 9.7 divisions, Figure 4G), confirming that *SIR2* was required for *MCD1* in
486 regulating RLS. Interestingly, the *sir2*Δ *hst1*Δ *fob1*Δ *hmr*Δ quadruple mutant combination, which
487 suppressed CIN in aged cells (Figure 1H), fully restored RLS of the short lived *sir2*Δ *hst1*Δ
488 combination to WT levels (Figure 4G, p=n.s.), suggesting that CIN is a key driver of replicative
489 aging downstream of Sir2 and Hst1.
490 Considering the strong depletion of cohesin from rDNA in aged cells (Figure 2D), and
491 extended RLS when *MCD1* was overexpressed (Figure 4E), we next tested if age-induced rDNA
492 instability was suppressed by *MCD1* overexpression using a reporter strain harboring *ADE2* in
493 the rDNA array (KAEBERLEIN *et al.* 1999). There was a large increase of red/white ½ sectoring
494 (marker loss) from aged cells that was suppressed upon *MCD1* overexpression (Figure 4H). In

495 the absence of *SIR2*, ½ sectoring was high from young and aged cells when the empty vector
496 (pRF10) was integrated, and *MCD1* overexpression did not significantly reduce rDNA instability
497 in either population (Figure 4H), indicating that at least some Sir2 was required for Mcd1 to
498 impact rDNA stability. We conclude that loss of Sir2 and cohesin in aging cells causes rDNA
499 array instability that generally exacerbates CIN.
500
501 **RLS extension by CR correlates with improved chromosome stability**
502 Reducing glucose concentration in the growth medium is effective at extending RLS and
503 is considered a form of caloric restriction (CR) for yeast (JIANG *et al.* 2000; LIN *et al.* 2002).
504 There have been several hypotheses put forth for the underlying mechanisms, including
505 stabilization of the rDNA, as CR suppresses recombination within the rDNA (LAMMING *et al.*
506 2005; RIESEN AND MORGAN 2009; SMITH *et al.* 2009). Since *MCD1* overexpression suppressed
507 rDNA recombination and extended RLS, we hypothesized that CR may suppress the abbreviated
508 RLS of a cohesin-depleted *mcd1L12STOP* mutant strain. Indeed, CR extended RLS of both the
509 WT and *mcd1L12STOP* strains (Figure 5A, $p<0.01$ and $p<1.0x10^{-7}$ respectively). However, the
510 suppression was apparently not due to maintenance of global cohesin levels because steady state
511 Mcd1-13xMyc was still depleted in glucose restricted aged cells (Figure 5B). CR also strongly
512 suppressed minichromosome loss in young and aged cells, even in the *sir2*Δ *hst1*Δ double mutant
513 (Figure 5C). Importantly, this CR effect also correlated with almost complete rescue of RLS for
514 the *sir2*Δ *hst1*Δ mutant (Figure 5D, p=n.s.). Taken together, the results support a mechanism for
515 RLS extension by CR, whereby stabilization of the rDNA locus helps maintain general mitotic
516 chromosome stability to protect against aneuploidy.
517

518 **The rDNA array has an opportunity to interact with centromeres during anaphase**

519 To conclude this study, we asked whether there is any mechanistic connection between
520 the rDNA and centromeres that could cause CIN. If rDNA instability has a direct effect on SCC
521 during aging, then we should observe elevated dissociation of sister chromatids in a *sir2*Δ mutant
522 and improved SCC in a *fob1*Δ mutant. However, as shown in Figure S7, the frequency of 2 GFP
523 dots in the SCC assay for these two mutants in aged populations was comparable to WT (see
524 Figure 3E and F). Alternatively, the rDNA could potentially affect centromere function through
525 direct contacts. Previous Hi-C analysis of the yeast genome and fluorescence microscopy of
526 nucleolar proteins positioned the rDNA off to one side of the nucleus, apparently secluded from
527 the rest of the genome (GOTTA *et al.* 1997; DUAN *et al.* 2010). The repetitive nature of rDNA
528 precludes it from appearing in Hi-C contact maps, but closer inspection of iteratively corrected
529 chromosome XII contact maps at 10 kb resolution indicated a clear interaction between unique
530 sequences flanking the centromere-proximal (left) edge of the array and *CEN12* (Figure 6A,
531 yellow arrow). We hypothesized that this contact was regulated by Sir2 since it is in the vicinity
532 of a known tRNA boundary (tQ(UUG)L) for rDNA silencing (BISWAS *et al.* 2009), but deletion
533 of *SIR2* had no effect on the contact (data not shown). Interestingly, all centromeres of the yeast
534 genome, including *CEN12*, cluster together in asynchronous cell population Hi-C data (Figure
535 6B, yellow arrows; (DUAN *et al.* 2010)), which potentially places them in proximity with the
536 rDNA given the association of *CEN12* with sequences flanking the rDNA. During anaphase, the
537 rDNA is thought to be separated from centromeres, but analysis of Hi-C data for cell-cycle
538 synchronized *cdc15-2*, which arrests cells in anaphase, revealed that the rDNA-proximal/*CEN12*
539 contact specifically occurs during anaphase (Figure 6C, (LAZAR-STEFANITA *et al.* 2017)), during
540 which time the centromeres are still clustered together by the spindle pole body (Figure 6D).

541 Taken together, these results suggest that the rDNA may transiently contact the centromeres
542 during mitosis, providing a potential window of time for a destabilized rDNA array to negatively
543 impact the integrity of general chromosome segregation during mitosis (Figure 6E).
544

545 Discussion

546 Nuclear protein depletion during replicative aging as a paradigm for aging pathologies

547 During this study the majority of chromatin-associated proteins that we analyzed by
548 western blotting were depleted in replicatively aged yeast cells. The only protein unaffected by
549 age that we tested, other than the vacuolar Vma2 control, was Sir3 (Figure 1D). A similar
550 proportion of homologous recombination proteins were depleted in an independent analysis of
551 aged cells, with Rad52 the only one tested that was not affected (PAL *et al.* 2018). These results
552 suggest there is at least some selectivity to the depletion of nuclear proteins in aged cells.
553 However, the large number of depleted factors also makes it likely that targeted nuclear protein
554 deficiency could lead to multiple age-associated phenotypes. Replicatively aging yeast cells
555 appear especially susceptible to this phenomenon, as even total core histone levels are depleted
556 (HU *et al.* 2014). Evidence also exists for histone depletion during aging of metazoan organisms,
557 including mammals (reviewed in (SONG AND JOHNSON 2018)). More generally, global protein
558 turnover is elevated in cells from prematurely aging progeria patients, which may trigger higher
559 translation rates (BUCHWALTER AND HETZER 2017). This is significant because reducing
560 translation is a means of extending lifespan in multiple organisms (MEHTA *et al.* 2010). The
561 mechanism(s) driving nuclear protein depletion in aged yeast mother cells or other organisms
562 remain unclear.

563 The specificity for Sir2/Sir4 depletion over Sir3 is intriguing given that Sir2 and Sir4
564 form a tight complex that allosterically stimulates the deacetylase activity of Sir2 (HSU *et al.*
565 2013), while Sir3 is a subunit of the SIR holocomplex (OPPIKOFER *et al.* 2011). Since Sir3 levels
566 are elevated in aged cells (Figure 1D; (JANSSENS *et al.* 2015)), it is likely to have a function
567 independent of the SIR complex during aging. The mechanism for Sir2/Sir4 depletion from aged
568 cells remains uncharacterized, though in non-aging cell populations the stability/turnover of Sir4,
569 but not Sir2, is mediated by the E3 ubiquitin ligase San1 (DASGUPTA *et al.* 2004), which has also
570 been implicated as a quality control E3 ligase for mutated/unfolded nuclear proteins (GARDNER
571 *et al.* 2005). Whether San1 controls Sir4 stability during aging remains unknown, but since Sir4
572 is more severely depleted than Sir2 in aged cells (Figures 1A and 2C), Sir4 could be selectively
573 depleted from the SIR complex, thus leaving Sir2 unprotected and subject to turnover through a
574 different mechanism. Consistent with this idea, we note that Sir4 is depleted independently of
575 Sir2 during extended G1 arrest (LARIN *et al.* 2015). Alternatively, Sir2/Sir4 could be equally
576 depleted as a complex from telomeres and the *HM* loci (not necessarily via San1), leaving the
577 nucleolar pool of Sir2/RENT as more resistant to aging. Under this scenario, protecting integrity
578 of the rDNA array could take precedence over other heterochromatic domains. Interestingly, the
579 *Schizosaccharomyces pombe* San1 ortholog has also been implicated in a chaperone-assisted
580 degradation pathway that functions in quality control of kinetochores to promote chromosome
581 stability (KRIEGENBURG *et al.* 2014).
582 Sir2 depletion in replicatively aged yeast cells is reminiscent of Sirt1 depletion in serially
583 passaged mouse embryonic fibroblasts (MEFs), which correlates with declining mitotic activity
584 (SASAKI *et al.* 2006). Sir2 and Sirt1 are both known to function in regulating DNA replication
585 origins (HOGGARD *et al.* 2018; UTANI AND ALADJEM 2018), and the effect of deleting *SIR2* on

586 early origin firing is thought to be mediated by competition for limiting factors with the repeated
587 rDNA origins (YOSHIDA *et al.* 2014). Furthermore, CR has been proposed to extend RLS by
588 reducing rDNA origin firing, which improves overall genome replication (KWAN *et al.* 2013).
589 This may help explain why CR can extend RLS and suppress CIN even when *SIR2* and *HST1* are
590 deleted. Conversely, depleted cohesin in old cells could potentially cause rDNA instability by
591 impacting DNA replication and repair.
592
593 **A precarious balance between rDNA and centromeric cohesin**
594 SCC ensures chromosomes are not segregated until the Mcd1/Scc1 cohesin subunit is
595 cleaved in response to a mitotic spindle checkpoint signal that all chromosomes are properly
596 attached to microtubules and aligned at the metaphase plate (reviewed in (MARSTON 2014)).
597 Cohesin is also critical during meiosis, and it is well established in mammals that SCC defects
598 occur in the oocytes of older mothers, causing meiotic chromosome missegregation events
599 during both anaphase I and II (JESSBERGER 2012). This phenomenon is believed to be a major
600 mechanism for increased aneuploidy risk that usually results in embryonic lethality, or in the
601 case of chromosome 21 trisomy, Down's syndrome. The meiotic cohesin subunit Rec8 is
602 depleted in the oocytes of older mice, as is Shugoshin (Sgo2), which normally protects/maintains
603 centromeric cohesin (LISTER *et al.* 2010). More recent experiments in *Drosophila* suggest that
604 oxidative stress in aged oocytes contributes to the SCC defects (PERKINS *et al.* 2016). Our results
605 in replicatively aging yeast cells reveal that aging-induced cohesin depletion and the resulting
606 chromosome missegregation can extend to mitotic cells. Though cohesin depletion or defects
607 have not been reported for aging mammalian somatic cells, the mitotic spindle checkpoint
608 protein BubR1 is depleted in dynamic somatic tissues such as spleen in aged mice (BAKER *et al.*

609 2004). Deficiency of this protein results in premature aging phenotypes (BAKER *et al.* 2004),
610 while overexpression extends lifespan (BAKER *et al.* 2013). This is similar to the effects we
611 observe with Mcd1 depletion and overexpression on yeast RLS. Interestingly, BubR1 is also a
612 deacetylation target of Sirt2, which appears to stabilize the protein and extend lifespan, thus
613 linking mitotic spindle checkpoint regulation to NAD^+ metabolism (NORTH *et al.* 2014). It
614 remains unclear if Sir2, Hst1, or other sirtuins regulate the yeast BubR1 ortholog, Mad3, or
615 additional checkpoint and kinetochore proteins.

616 SCC is the canonical function for cohesin, though the complex also functions in
617 establishing and regulating genome organization at the level of chromatin structure, gene
618 regulation, and double strand break (DSB) repair (reviewed in (UHLMANN 2016)). Among these
619 various processes, SCC at centromeres appears the most critical because artificial depletion of
620 Mcd1 to <30% of normal levels results in preferential cohesin binding to pericentromeric regions
621 rather than cohesin associated regions (CARs) on chromosome arms (HEIDINGER-PAULI *et al.*
622 2010). SCC was also well maintained in these strains at the expense of normal chromosome
623 condensation, DNA repair, and rDNA stability (HEIDINGER-PAULI *et al.* 2010). In aged yeast
624 cells, we observed relative enrichment of Mcd1-myc at centromeres as compared to loss at the
625 rDNA (IGS1) locus (Figures 2D and 2E) consistent with pericentromeric cohesin retention in the
626 artificially depleted system. Despite maintaining the cohesin complex at centromeres, SCC was
627 still slightly impaired in the aged cells, but only if we analyzed cells >7 generations old. We
628 suspect cohesin was reduced at centromeres in these older cells, which would be consistent with
629 the loss of centromeric Mcd1 enrichment when cells were aged longer for 36 hr, but it was also
630 likely that some of the centromere-localized Mcd1 was non-functional. These results are in line
631 with an independent study that analyzed significantly older mother cells (~25 generations) and

632 observed reduced cohesin enrichment at centromeres and severe loss of SCC (PAL *et al.* 2018).
633 Another recent study using single cell microfluidics found that chromosome loss was very
634 common just prior to the last cell division (NEUROHR *et al.* 2018). Collectively, the results
635 suggest that centromere-associated cohesin is preferentially retained during the initial stages of
636 replicative aging, but then eventually breaks down below a critical threshold in the oldest cells.
637 Numerous nuclear proteins are depleted in aged yeast cells, not just cohesin subunits, so
638 we hypothesize that defects in other nuclear processes mediated by such factors also contribute
639 to SCC defects and chromosome instability either directly or indirectly. The depleted cohesin
640 loading complex (Scc2/4) is an obvious candidate due to its role in loading cohesin at
641 centromeres and CARs. Similarly, the depleted cohibin complex (Figure S2) is proposed to act as
642 a cohesin clamp onto rDNA chromatin (HUANG *et al.* 2006), and also functions at centromeres to
643 maintain mitotic integrity (BITTO *et al.* 2015). Sir2 and Hst1 are also obvious candidates given
644 the earlier finding that H4K16 deacetylation at centromeres by Sir2 helps maintain chromosome
645 stability (CHOY *et al.* 2011). Part of this effect is apparently due to the pseudo-diploid phenotype
646 of a *sir2*Δ mutation, which has been previously shown to impact RLS (KAEBERLEIN *et al.* 1999).
647 Hst1 also binds centromeric DNA *in vitro* and *in vivo* (OHKUNI AND KITAGAWA 2011), though
648 the functional relevance of that association remains uncharacterized. The suppression of age-
649 associated mini-chromosome loss in the absence of *FOB1* clearly points to rDNA instability as
650 an unexpected source of general CIN. Such a relationship is reinforced by the observed depletion
651 of nucleolar proteins Net1 and Lrs4 in aged cells (Figures 2E and S2), both of which are required
652 for normal rDNA/nucleolar integrity and stable cohesin association with the rDNA (SMITH *et al.*
653 1999; STRAIGHT *et al.* 1999; HUANG *et al.* 2006).

654 How could destabilization of the rDNA locus result in general chromosome instability
655 and shortened RLS? As depicted in Figure 6, unique sequence flanking the rDNA contacts the
656 centromere of chromosome XII, thus placing it in proximity to other centromeres during
657 anaphase. Whether the actual rDNA genes contact centromeres remains unclear due to the
658 current limitations of Hi-C analysis with repetitive DNA. However, specific regions of the rDNA
659 were previously shown to associate with various non-rDNA chromosomal regions using an
660 anchored 4C approach (O'SULLIVAN *et al.* 2009). Furthermore, multiple nucleolar associated
661 domains have been identified in metazoan cells that copurify with nucleoli (MATHESON AND
662 KAUFMAN 2016). Loss of cohesin from the rDNA could potentially disrupt long-range
663 interactions with centromeres or non-centromeric regions of cohesin association that influence
664 chromosome integrity. One potential mechanism could be significant disruption of overall
665 chromosome condensation during mitosis, as cohesin appears to play a larger role in the DNA
666 looping associated with chromosome condensation in budding yeast than previously thought
667 (SCHALBETTER *et al.* 2017).
668 Interestingly, another class of nuclear factors depleted in aged yeast cells are several
669 DNA repair proteins (PAL *et al.* 2018). Consequently, the lack of proper DNA repair while the
670 rDNA becomes destabilized correlates with fragmentation of chromosome XII and the other
671 chromosomes (PAL *et al.* 2018). Rad52 foci also appear in aged cells indicating persistent DNA
672 damage (NEUROHR *et al.* 2018). It was proposed that accumulation of breaks and rearrangements
673 ultimately causes cell death during replicative aging. Such cells were significantly older (>25
674 divisions) compared to the cells in our study, which exhibited a maximum of 13 divisions after
675 24 hr. Alternatively, it is possible that these presumably random rearrangements disrupt normal
676 SCC, leading to CIN.

677

678 **Aneuploidy as an aging mechanism**

679 All 16 *S. cerevisiae* chromosomes harbor essential genes, so if a single chromosome is
680 lost from a haploid yeast cell, then the affected mother or daughter cell should become inviable
681 and no longer divide. Given the elevated frequency of chromosome loss during replicative aging,
682 the chances of generating an inviable mother cell during a replicative aging assay increases after
683 each subsequent division. Therefore, at least a portion of the replicative lifespan in haploid yeast
684 cells is controlled by the ability to maintain all 16 chromosomes. Complete loss of a
685 chromosome would not be an immediate viability issue for diploid cells, however, due to the
686 chances of losing both homologs in a single mitosis being exceedingly rare. On the other hand,
687 haploid strains that are disomic for individual chromosomes are often short lived, with longer
688 chromosomes typically having larger effects (SUNSHINE *et al.* 2016). It was hypothesized that
689 such strains suffer from proteotoxic stress due to inappropriate protein expression levels.
690 Therefore, a similar mechanism could shorten RLS in a diploid strain that is trisomic for an
691 individual chromosome, though this has not yet been tested. Aneuploidy is also a hallmark of
692 aging in the germline (NAGAOKA *et al.* 2012), and somatic tissues of mammals (LUSHNIKOVA *et*
693 *al.* 2011; BAKER *et al.* 2013), making it a conserved feature of aging from yeast to humans.

694 Another exciting feature of this study is the suppression of CIN by CR growth conditions
695 that extend RLS. This effect was independent of the reduced cohesin levels in aged cells, and
696 even improved RLS of the cohesin-depleted strains. Since SCC is normal in the cohesin-depleted
697 strain (HEIDINGER-PAULI *et al.* 2010), we hypothesize that CR reinforces other processes that are
698 defective due to reduced cohesin or other depleted factors that promote rDNA stability. Indeed,
699 CR is known to suppress rDNA instability in yeast cells (RIESEN AND MORGAN 2009; SMITH *et*

700 *al.* 2009), and improve overall genome replication efficiency (KWAN *et al.* 2013). Hi-C analysis
701 also suggests there could be direct effects of rDNA structure on centromere function, which will
702 be a focus of future investigation.
703

704 ## Acknowledgments

705 We thank Dan Gottschling and all lab members for kindly providing yeast strains and initial
706 advice on the MEP system. Stefan Bekiranov, Job Dekker, Jon Belton, Maitreya Dunham, Ivan
707 Liachko, Maxim Imakev, and Anton Goloborodko all provided valuable advice on Hi-C
708 protocols and analysis methods. We thank Doug Koshland for providing the Mcd1 reduction and
709 cohesion assay strains, and Matt Kaeberlein for rDNA marker loss strains. We also thank Jef
710 Boeke, Marc Gartenberg, and Dan Gottschling for providing antibodies. Special thanks to Todd
711 Stukenberg for microscopy assistance. Lastly, thanks to David Auble for critically reading the
712 manuscript and providing comments prior to submission. We declare no conflicts of interest.
713

714 ## References

715 Ausubel, F. M., R. Brent, R. E. Kingston, D. D. Moore, J. G. Seidman *et al.* (Editors), 2000
716 *Current Protocols in Molecular Biology*. John Wiley & Sons, Inc., New York.
717 Baker, D. J., M. M. Dawlaty, T. Wijshake, K. B. Jeganathan, L. Malureanu *et al.*, 2013 Increased
718 expression of BubR1 protects against aneuploidy and cancer and extends healthy
719 lifespan. Nat Cell Biol 15**:** 96-102.
720 Baker, D. J., K. B. Jeganathan, J. D. Cameron, M. Thompson, S. Juneja *et al.*, 2004 BubR1
721 insufficiency causes early onset of aging-associated phenotypes and infertility in mice.
722 Nat Genet 36**:** 744-749.

723 Belli, G., E. Gari, L. Piedrafita, M. Aldea and E. Herrero, 1998 An activator/repressor dual
724 system allows tight tetracycline-regulated gene expression in budding yeast. Nucleic
725 Acids Res 26**:** 942-947.
726 Belton, J. M., and J. Dekker, 2015 Measuring chromatin structure in budding yeast. Cold Spring
727 Harb Protoc 2015**:** 614-618.
728 Biswas, M., N. Maqani, R. Rai, S. P. Kumaran, K. R. Iyer *et al.*, 2009 Limiting the extent of the
729 *RDN1* heterochromatin domain by a silencing barrier and Sir2 protein levels in
730 *Saccharomyces cerevisiae*. Mol Cell Biol 29**:** 2889-2898.
731 Bitto, A., A. M. Wang, C. F. Bennett and M. Kaeberlein, 2015 Biochemical genetic pathways
732 that modulate aging in multiple species. Cold Spring Harb Perspect Med 5.
733 Brachmann, C. B., A. Davies, G. J. Cost, E. Caputo, J. Li *et al.*, 1998 Designer deletion strains
734 derived from *Saccharomyces cerevisiae* S288C: a useful set of strains and plasmids for
735 PCR-mediated gene disruption and other applications. Yeast 14**:** 115-132.
736 Brachmann, C. B., J. M. Sherman, S. E. Devine, E. E. Cameron, L. Pillus *et al.*, 1995 The *SIR2*
737 gene family, conserved from bacteria to humans, functions in silencing, cell cycle
738 progression, and chromosome stability. Genes Dev 9**:** 2888-2902.
739 Bryk, M., M. Banerjee, M. Murphy, K. E. Knudsen, D. J. Garfinkel *et al.*, 1997 Transcriptional
740 silencing of Ty1 elements in the *RDN1* locus of yeast. Genes Dev 11**:** 255-269.
741 Buchwalter, A., and M. W. Hetzer, 2017 Nucleolar expansion and elevated protein translation in
742 premature aging. Nat Commun 8**:** 328.
743 Buck, S. W., C. M. Gallo and J. S. Smith, 2004 Diversity in the Sir2 family of protein
744 deacetylases. J Leukoc Biol 75**:** 939-950.

745 Buck, S. W., J. J. Sandmeier and J. S. Smith, 2002 RNA polymerase I propagates unidirectional
746 spreading of rDNA silent chromatin. Cell 111**:** 1003-1014.
747 Burton, J. N., I. Liachko, M. J. Dunham and J. Shendure, 2014 Species-level deconvolution of
748 metagenome assemblies with Hi-C-based contact probability maps. G3 (Bethesda) 4**:**
749 1339-1346.
750 Chang, C. R., C. S. Wu, Y. Hom and M. R. Gartenberg, 2005 Targeting of cohesin by
751 transcriptionally silent chromatin. Genes Dev 19**:** 3031-3042.
752 Choy, J. S., R. Acuna, W. C. Au and M. A. Basrai, 2011 A role for histone H4K16
753 hypoacetylation in *Saccharomyces cerevisiae* kinetochore function. Genetics 189**:** 11-21.
754 Ciosk, R., M. Shirayama, A. Shevchenko, T. Tanaka, A. Toth *et al.*, 2000 Cohesin's binding to
755 chromosomes depends on a separate complex consisting of Scc2 and Scc4 proteins. Mol
756 Cell 5**:** 243-254.
757 Dang, W., K. K. Steffen, R. Perry, J. A. Dorsey, F. B. Johnson *et al.*, 2009 Histone H4 lysine 16
758 acetylation regulates cellular lifespan. Nature 459**:** 802-807.
759 Dasgupta, A., K. L. Ramsey, J. S. Smith and D. T. Auble, 2004 Sir Antagonist 1 (San1) is a
760 ubiquitin ligase. J Biol Chem 279**:** 26830-26838.
761 Defossez, P. A., R. Prusty, M. Kaeberlein, S. J. Lin, P. Ferrigno *et al.*, 1999 Elimination of
762 replication block protein Fob1 extends the life span of yeast mother cells. Mol Cell 3**:**
763 447-455.
764 Derbyshire, M. K., K. G. Weinstock and J. N. Strathern, 1996 *HST1*, a new member of the *SIR2*
765 family of genes. Yeast 12**:** 631-640.
766 Duan, Z., M. Andronescu, K. Schutz, S. McIlwain, Y. J. Kim *et al.*, 2010 A three-dimensional
767 model of the yeast genome. Nature 465**:** 363-367.

768 Ganley, A. R., and T. Kobayashi, 2014 Ribosomal DNA and cellular senescence: new evidence
769 supporting the connection between rDNA and aging. FEMS Yeast Res 14**:** 49-59.
770 Gardner, R. G., Z. W. Nelson and D. E. Gottschling, 2005 Degradation-mediated protein quality
771 control in the nucleus. Cell 120**:** 803-815.
772 Gartenberg, M. R., and J. S. Smith, 2016 The nuts and bolts of transcriptionally silent chromatin
773 in *Saccharomyces cerevisiae*. Genetics 203**:** 1563-1599.
774 Gomes, A. P., N. L. Price, A. J. Ling, J. J. Moslehi, M. K. Montgomery *et al.*, 2013 Declining
775 NAD^+ induces a pseudohypoxic state disrupting nuclear-mitochondrial communication
776 during aging. Cell 155**:** 1624-1638.
777 Gotta, M., S. Strahl-Bolsinger, H. Renauld, T. Laroche, B. K. Kennedy *et al.*, 1997 Localization
778 of Sir2p: the nucleolus as a compartment for silent information regulators. EMBO J 16**:**
779 3243-3255.
780 Guacci, V., and D. Koshland, 2012 Cohesin-independent segregation of sister chromatids in
781 budding yeast. Mol Biol Cell 23**:** 729-739.
782 Guacci, V., D. Koshland and A. Strunnikov, 1997 A direct link between sister chromatid
783 cohesion and chromosome condensation revealed through the analysis of *MCD1* in *S.*
784 *cerevisiae*. Cell 91**:** 47-57.
785 Heidinger-Pauli, J. M., O. Mert, C. Davenport, V. Guacci and D. Koshland, 2010 Systematic
786 reduction of cohesin differentially affects chromosome segregation, condensation, and
787 DNA repair. Curr Biol 20**:** 957-963.
788 Hickman, M. A., and L. N. Rusche, 2007 Substitution as a mechanism for genetic robustness: the
789 duplicated deacetylases Hst1p and Sir2p in *Saccharomyces cerevisiae*. PLoS Genet 3**:**
790 e126.

791 Hoggard, T. A., F. Chang, K. R. Perry, S. Subramanian, J. Kenworthy *et al.*, 2018 Yeast
792 heterochromatin regulators Sir2 and Sir3 act directly at euchromatic DNA replication
793 origins. PLoS Genet 14**:** e1007418.
794 Hsu, H. C., C. L. Wang, M. Wang, N. Yang, Z. Chen *et al.*, 2013 Structural basis for allosteric
795 stimulation of Sir2 activity by Sir4 binding. Genes Dev 27**:** 64-73.
796 Hu, Z., K. Chen, Z. Xia, M. Chavez, S. Pal *et al.*, 2014 Nucleosome loss leads to global
797 transcriptional up-regulation and genomic instability during yeast aging. Genes Dev 28**:**
798 396-408.
799 Huang, J., I. L. Brito, J. Villen, S. P. Gygi, A. Amon *et al.*, 2006 Inhibition of homologous
800 recombination by a cohesin-associated clamp complex recruited to the rDNA
801 recombination enhancer. Genes Dev 20**:** 2887-2901.
802 Janssens, G. E., A. C. Meinema, J. Gonzalez, J. C. Wolters, A. Schmidt *et al.*, 2015 Protein
803 biogenesis machinery is a driver of replicative aging in yeast. Elife 4**:** e08527.
804 Jessberger, R., 2012 Age-related aneuploidy through cohesion exhaustion. EMBO Rep 13**:** 539-
805 546.
806 Jiang, J. C., E. Jaruga, M. V. Repnevskaya and S. M. Jazwinski, 2000 An intervention
807 resembling caloric restriction prolongs life span and retards aging in yeast. FASEB J 14**:**
808 2135-2137.
809 Kaeberlein, M., M. McVey and L. Guarente, 1999 The SIR2/3/4 complex and SIR2 alone
810 promote longevity in *Saccharomyces cerevisiae* by two different mechanisms. Genes Dev
811 13**:** 2570-2580.
812 Kobayashi, T., and A. R. Ganley, 2005 Recombination regulation by transcription-induced
813 cohesin dissociation in rDNA repeats. Science 309**:** 1581-1584.

814 Kobayashi, T., and T. Horiuchi, 1996 A yeast gene product, Fob1 protein, required for both
815 replication fork blocking and recombinational hotspot activities. Genes Cells 1**:** 465-474.
816 Kobayashi, T., T. Horiuchi, P. Tongaonkar, L. Vu and M. Nomura, 2004 *SIR2* regulates
817 recombination between different rDNA repeats, but not recombination within individual
818 rRNA genes in yeast. Cell 117**:** 441-453.
819 Kogut, I., J. Wang, V. Guacci, R. K. Mistry and P. C. Megee, 2009 The Scc2/Scc4 cohesin
820 loader determines the distribution of cohesin on budding yeast chromosomes. Genes Dev
821 23**:** 2345-2357.
822 Kriegenburg, F., V. Jakopec, E. G. Poulsen, S. V. Nielsen, A. Roguev *et al.*, 2014 A chaperone-
823 assisted degradation pathway targets kinetochore proteins to ensure genome stability.
824 PLoS Genet 10**:** e1004140.
825 Kwan, E. X., E. J. Foss, S. Tsuchiyama, G. M. Alvino, L. Kruglyak *et al.*, 2013 A natural
826 polymorphism in rDNA replication origins links origin activation with calorie restriction
827 and lifespan. PLoS Genet 9**:** e1003329.
828 Lamming, D. W., M. Latorre-Esteves, O. Medvedik, S. N. Wong, F. A. Tsang *et al.*, 2005 *HST2*
829 mediates *SIR2*-independent life-span extension by calorie restriction. Science 309**:** 1861-
830 1864.
831 Larin, M. L., K. Harding, E. C. Williams, N. Lianga, C. Dore *et al.*, 2015 Competition between
832 heterochromatic loci allows the abundance of the silencing protein, Sir4, to regulate *de*
833 *novo* assembly of heterochromatin. PLoS Genet 11**:** e1005425.
834 Lazar-Stefanita, L., V. F. Scolari, G. Mercy, H. Muller, T. M. Guerin *et al.*, 2017 Cohesins and
835 condensins orchestrate the 4D dynamics of yeast chromosomes during the cell cycle.
836 EMBO J 36**:** 2684-2697.

837 Li, C., J. E. Mueller and M. Bryk, 2006 Sir2 represses endogenous polymerase II transcription
838 units in the ribosomal DNA nontranscribed spacer. Mol Biol Cell 17**:** 3848-3859.
839 Li, M., B. J. Petteys, J. M. McClure, V. Valsakumar, S. Bekiranov *et al.*, 2010 Thiamine
840 biosynthesis in *Saccharomyces cerevisiae* is regulated by the NAD^+-dependent histone
841 deacetylase Hst1. Mol Cell Biol 30**:** 3329-3341.
842 Li, M., V. Valsakumar, K. Poorey, S. Bekiranov and J. S. Smith, 2013 Genome-wide analysis of
843 functional sirtuin chromatin targets in yeast. Genome Biol 14**:** R48.
844 Lin, S. J., M. Kaeberlein, A. A. Andalis, L. A. Sturtz, P. A. Defossez *et al.*, 2002 Calorie
845 restriction extends *Saccharomyces cerevisiae* lifespan by increasing respiration. Nature
846 418**:** 344-348.
847 Lindstrom, D. L., and D. E. Gottschling, 2009 The mother enrichment program: a genetic system
848 for facile replicative life span analysis in *Saccharomyces cerevisiae*. Genetics 183**:** 413-
849 422, 411si-413si.
850 Lindstrom, D. L., C. K. Leverich, K. A. Henderson and D. E. Gottschling, 2011 Replicative age
851 induces mitotic recombination in the ribosomal RNA gene cluster of *Saccharomyces*
852 *cerevisiae*. PLoS Genet 7**:** e1002015.
853 Lister, L. M., A. Kouznetsova, L. A. Hyslop, D. Kalleas, S. L. Pace *et al.*, 2010 Age-related
854 meiotic segregation errors in mammalian oocytes are preceded by depletion of cohesin
855 and Sgo2. Curr Biol 20**:** 1511-1521.
856 Lushnikova, T., A. Bouska, J. Odvody, W. D. Dupont and C. M. Eischen, 2011 Aging mice have
857 increased chromosome instability that is exacerbated by elevated Mdm2 expression.
858 Oncogene 30**:** 4622-4631.

859 Marston, A. L., 2014 Chromosome segregation in budding yeast: sister chromatid cohesion and
860 related mechanisms. Genetics 196**:** 31-63.
861 Matecic, M., D. L. Smith, X. Pan, N. Maqani, S. Bekiranov *et al.*, 2010 A microarray-based
862 genetic screen for yeast chronological aging factors. PLoS Genet 6**:** e1000921.
863 Matheson, T. D., and P. D. Kaufman, 2016 Grabbing the genome by the NADs. Chromosoma
864 125**:** 361-371.
865 Mehta, R., D. Chandler-Brown, F. J. Ramos, L. S. Shamieh and M. Kaeberlein, 2010 Regulation
866 of mRNA translation as a conserved mechanism of longevity control. Adv Exp Med Biol
867 694**:** 14-29.
868 Moazed, D., A. Kistler, A. Axelrod, J. Rine and A. D. Johnson, 1997 Silent information regulator
869 protein complexes in *Saccharomyces cerevisiae*: a SIR2/SIR4 complex and evidence for
870 a regulatory domain in SIR4 that inhibits its interaction with SIR3. Proc Natl Acad Sci U
871 S A 94**:** 2186-2191.
872 Mortimer, R. K., and J. R. Johnston, 1959 Life span of individual yeast cells. Nature 183**:** 1751-
873 1752.
874 Nagaoka, S. I., T. J. Hassold and P. A. Hunt, 2012 Human aneuploidy: mechanisms and new
875 insights into an age-old problem. Nat Rev Genet 13**:** 493-504.
876 Neurohr, G. E., R. L. Terry, A. Sandikci, K. Zou, H. Li *et al.*, 2018 Deregulation of the G1/S-
877 phase transition is the proximal cause of mortality in old yeast mother cells. Genes Dev
878 32**:** 1075-1084.
879 North, B. J., M. A. Rosenberg, K. B. Jeganathan, A. V. Hafner, S. Michan *et al.*, 2014 SIRT2
880 induces the checkpoint kinase BubR1 to increase lifespan. Embo j 33**:** 1438-1453.

881 O'Sullivan, J. M., D. M. Sontam, R. Grierson and B. Jones, 2009 Repeated elements coordinate
882 the spatial organization of the yeast genome. Yeast 26**:** 125-138.
883 Ohkuni, K., and K. Kitagawa, 2011 Endogenous transcription at the centromere facilitates
884 centromere activity in budding yeast. Curr Biol 21**:** 1695-1703.
885 Oppikofer, M., S. Kueng, F. Martino, S. Soeroes, S. M. Hancock *et al.*, 2011 A dual role of
886 H4K16 acetylation in the establishment of yeast silent chromatin. EMBO J 30**:** 2610-
887 2621.
888 Pal, S., S. D. Postnikoff, M. Chavez and J. K. Tyler, 2018 Impaired cohesion and homologous
889 recombination during replicative aging in budding yeast. Sci Adv 4**:** eaaq0236.
890 Perkins, A. T., T. M. Das, L. C. Panzera and S. E. Bickel, 2016 Oxidative stress in oocytes
891 during midprophase induces premature loss of cohesion and chromosome segregation
892 errors. Proc Natl Acad Sci U S A 113**:** E6823-e6830.
893 Riesen, M., and A. Morgan, 2009 Calorie restriction reduces rDNA recombination independently
894 of rDNA silencing. Aging Cell 8**:** 624-632.
895 Rine, J., and I. Herskowitz, 1987 Four genes responsible for a position effect on expression from
896 *HML* and *HMR* in *Saccharomyces cerevisiae*. Genetics 116**:** 9-22.
897 Sasaki, T., B. Maier, A. Bartke and H. Scrable, 2006 Progressive loss of SIRT1 with cell cycle
898 withdrawal. Aging Cell 5**:** 413-422.
899 Schalbetter, S. A., A. Goloborodko, G. Fudenberg, J. M. Belton, C. Miles *et al.*, 2017 SMC
900 complexes differentially compact mitotic chromosomes according to genomic context.
901 Nat Cell Biol 19**:** 1071-1080.

902 Schlissel, G., M. K. Krzyzanowski, F. Caudron, Y. Barral and J. Rine, 2017 Aggregation of the
903 Whi3 protein, not loss of heterochromatin, causes sterility in old yeast cells. Science 355**:**
904 1184-1187.
905 Shou, W., J. H. Seol, A. Shevchenko, C. Baskerville, D. Moazed *et al.*, 1999 Exit from mitosis is
906 triggered by Tem1-dependent release of the protein phosphatase Cdc14 from nucleolar
907 RENT complex. Cell 97**:** 233-244.
908 Sinclair, D. A., and L. Guarente, 1997 Extrachromosomal rDNA circles--a cause of aging in
909 yeast. Cell 91**:** 1033-1042.
910 Smeal, T., J. Claus, B. Kennedy, F. Cole and L. Guarente, 1996 Loss of transcriptional silencing
911 causes sterility in old mother cells of *S. cerevisiae*. Cell 84**:** 633-642.
912 Smith, D. L., Jr., C. Li, M. Matecic, N. Maqani, M. Bryk *et al.*, 2009 Calorie restriction effects
913 on silencing and recombination at the yeast rDNA. Aging Cell 8**:** 633-642.
914 Smith, J. S., and J. D. Boeke, 1997 An unusual form of transcriptional silencing in yeast
915 ribosomal DNA. Genes Dev 11**:** 241-254.
916 Smith, J. S., C. B. Brachmann, L. Pillus and J. D. Boeke, 1998 Distribution of a limited Sir2
917 protein pool regulates the strength of yeast rDNA silencing and is modulated by Sir4p.
918 Genetics 149**:** 1205-1219.
919 Smith, J. S., E. Caputo and J. D. Boeke, 1999 A genetic screen for ribosomal DNA silencing
920 defects identifies multiple DNA replication and chromatin-modulating factors. Mol Cell
921 Biol 19**:** 3184-3197.
922 Song, S., and F. B. Johnson, 2018 Epigenetic mechanisms impacting aging: a focus on histone
923 levels and telomeres. Genes (Basel) 9: 201.

924 Spencer, F., S. L. Gerring, C. Connelly and P. Hieter, 1990 Mitotic chromosome transmission
925 fidelity mutants in *Saccharomyces cerevisiae*. Genetics 124**:** 237-249.
926 Steffen, K. K., B. K. Kennedy and M. Kaeberlein, 2009 Measuring replicative life span in the
927 budding yeast. J Vis Exp. 28: e1209.
928 Straight, A. F., W. Shou, G. J. Dowd, C. W. Turck, R. J. Deshaies *et al.*, 1999 Net1, a Sir2-
929 associated nucleolar protein required for rDNA silencing and nucleolar integrity. Cell 97**:**
930 245-256.
931 Sunshine, A. B., G. T. Ong, D. P. Nickerson, D. Carr, C. J. Murakami *et al.*, 2016 Aneuploidy
932 shortens replicative lifespan in *Saccharomyces cerevisiae*. Aging Cell 15**:** 317-324.
933 Takeuchi, Y., T. Horiuchi and T. Kobayashi, 2003 Transcription-dependent recombination and
934 the role of fork collision in yeast rDNA. Genes Dev 17**:** 1497-1506.
935 Uhlmann, F., 2016 SMC complexes: from DNA to chromosomes. Nat Rev Mol Cell Biol 17**:**
936 399-412.
937 Unal, E., J. M. Heidinger-Pauli, W. Kim, V. Guacci, I. Onn *et al.*, 2008 A molecular determinant
938 for the establishment of sister chromatid cohesion. Science 321**:** 566-569.
939 Utani, K., and M. I. Aladjem, 2018 Extra View: Sirt1 Acts as a gatekeeper of replication
940 initiation to preserve genomic stability. Nucleus 9**:** 261-267.
941 Wasko, B. M., and M. Kaeberlein, 2014 Yeast replicative aging: a paradigm for defining
942 conserved longevity interventions. FEMS Yeast Res 14**:** 148-159.
943 Winston, F., C. Dollard and S. L. Ricupero-Hovasse, 1995 Construction of a set of convenient
944 *Saccharomyces cerevisiae* strains that are isogenic to S288C. Yeast 11**:** 53-55.
945 Wood, A. J., A. F. Severson and B. J. Meyer, 2010 Condensin and cohesin complexity: the
946 expanding repertoire of functions. Nat Rev Genet 11**:** 391-404.

947 Wu, C. S., Y. F. Chen and M. R. Gartenberg, 2011 Targeted sister chromatid cohesion by Sir2.
948 PLoS Genet 7**:** e1002000.
949 Yoshida, K., J. Bacal, D. Desmarais, I. Padioleau, O. Tsaponina *et al.*, 2014 The histone
950 deacetylases Sir2 and Rpd3 act on ribosomal DNA to control the replication program in
951 budding yeast. Mol Cell 54**:** 691-697.
952 Zhu, J., D. Heinecke, W. A. Mulla, W. D. Bradford, B. Rubinstein *et al.*, 2015 Single-cell based
953 quantitative assay of chromosome transmission fidelity. G3 (Bethesda) 5**:** 1043-1056.
954

955 ## Figure Legends

956 **Figure 1. Depletion of Sir2 complexes and elevated chromosome instability in replicatively**
957 **aging cells. (A)** Western blot of Sir2 protein levels in young and aged cells. Vma2 serves as a
958 loading control. **(B)** Depiction of the SIR and RENT complexes, which share Sir2 as a catalytic
959 subunit. **(C, D)** Western blots of native Sir4 and Sir3. **(E, F)** Western blots of 13xMyc tagged
960 Sir2 paralog, Hst1, and the Net1 subunit of RENT. **(G)** Schematic of artificial chromosome loss
961 assay for ½ sectored colonies. **(H)** Quantification of sectoring frequency for young or aged cell
962 populations. Approximately 10,000 colonies were analyzed for each strain across several
963 biological replicates. *$p<0.05$, two-tailed student t-test. Bud scar counts are an average for each
964 enriched population. Qty: indicates the mean western signal of each protein relative to Vma2,
965 with the ratio for young cells set at 1.0 (n=3 biological replicates).

966 **Figure 2. Chromosome instability is linked to rDNA stability and cohesin redistribution**
967 **(A)** Schematic of the cohesin complex subunits. **(B)** Western blot of Mcd1-13xMyc and Smc1-
968 13xMyc from young and aged cells. **(C)** Western blot of 13xMyc tagged Scc2. **(D, E, F, G)**

969 ChIP-qPCR of Mcd1-13xMyc in young cells (black bars) and aged cells (gray bars) at the
970 indicated loci normalized to background signal in the *STE2* ORF. **(H)** ChIP-qPCR of Sir4-
971 13xMyc in young and aged cells normalized to an intergenic *PDC1* site that shows SIR complex
972 association (Li *et al.* 2013). **(I, J)** ChIP-qPCR of Mcd1-13xMyc from a time course of young, 24
973 hr, and 36 hr aged cells at indicated loci normalized to *STE2* background signal. Asterisks
974 indicate significant differences between young and aged cells ($p<0.05$).
975
976 **Figure 3. Sister chromatid cohesion is weakened in aged yeast cells. (A)** Representative
977 control images of arm cohesion in an *mcd1-1* mutant at permissive (25°C) and non-permissive
978 (37°C) temperatures. **(B)** Quantification of cohesion maintenance (1-dot) or loss (2-dots) from
979 100 *mcd1-1* cells. **(C)** Representative images of young (log-phase) or aged cells arrested with
980 nocodazole (Nz) and monitored for centromere or arm cohesion. **(D)** Quantifying cohesion loss
981 (2-dots) in cells with at least 7 bud scars. *$p<0.05$, two-tailed t-test ($n>50$ cells). Quantification
982 of cohesion loss for young and aged cells in the absence of nocodazole **(F)** Representative
983 images of nocodazole untreated cells. White scale bar represents 2 microns.
984
985 **Figure 4. Modulation of RLS and CIN by manipulating *MCD1* and *SIR2* expression levels.**
986 **(A)** Representative images of chromosome loss (sectoring) for WT (YPH278) cells grown
987 continuously in 2% glucose, galactose, or raffinose. **(B)** Quantification of half-sector colonies
988 shown in 4A. *$p<0.001$, two-tailed student t-test. **(C)** RLS assay of YPH278 cells growing on
989 rich YEP agar plates containing either 2% glucose, galactose, or raffinose. ($n=64$, each
990 condition; mean RLS = ♦ 18.9, ■ 9.2, ▲ 15.5) **(D)** Quantification of chromosome loss (1/2
991 sectors) for strains with an integrated tet^{On} empty (pRF10) or *MCD1* (pRF11) construct. RLS

992 assays of WT (*MCD1*$^{+}$) and *mcd1L12STOP* strains with integrated pRF10 or pRF11 constructs
993 (mean RLS = ♦16.2, ■ 10.3, ▲ 19.2, ×15.6). **(F)** RLS assay of WT and *mcd1L12STOP* strains
994 with integrated empty, pRS306, or *SIR2* containing plasmid, pJSB186 (n=40 cells each; mean
995 RLS = ♦21.5 ■ 9.9 ▲ 30.4 ×14.8). **(G)** RLS assay with *MCD1* OE or *fob1*Δ *hmr*Δ rescue of
996 *sir2*Δ or *sir2*Δ *hst1*Δ mutants (mean RLS = ♦16.5, ■ 10.1, ▲ 9.7, ×10.7, ∗ 10.25, ● 16.7). **(H)**
997 rDNA recombination (marker loss, ½ sector) assay with rDNA marker loss reporter strain
998 W303AR bearing *ADE2* within the rDNA array. (* p<0.05, two-tailed t-test).

999 **Figure 5. CR suppresses the CIN and RLS defects of *sir2*Δ and *mcd1* mutants**. **(A)** RLS
1000 assay of WT (JH5275b) and *mcd1L12STOP* (JH5276b) strains under normal 2% glucose and CR
1001 (0.5% glucose) conditions (n=32 cells; mean RLS = ♦21.3, ■ 8.1, ▲ 24.1, ×13.8). **(B)** Western
1002 blot of Mcd1-13xMyc for cultures grown in YEP media containing 0.5% glucose. **(C)**
1003 Chromosome loss (sectoring) assay of strains grown in media containing 0.5% glucose. Data
1004 from Figure 1H included for reference. *p<0.05, two-tailed t-test. **(D)** RLS assay of WT and
1005 *sir2Δhst1Δ* mutant strains under normal and CR conditions. (n=32 cells; mean rls = ♦19.6, ■
1006 9.3, ▲ 23.5, ×17.1).

1007 **Figure 6. Chromosomal instability during replicative aging is linked to the rDNA.**
1008 **(A)** Iteratively corrected and read-normalized heatmap of ChrXII Hi-C contact data at 10 kb
1009 resolution in WT cells growing asynchronously, revealing an interaction between *CEN12* (bin
1010 15) and unique sequence adjacent to the rDNA (bin 45), indicated by yellow arrow. **(B)** Contact
1011 heatmap of chromosomes XI, XII, and XIII showing centromere clustering in asynchronously
1012 growing WT cells. Yellow arrows indicate examples of centromere alignment with *CEN12* and

1013 sequence adjacent to the rDNA. **(C)** Iteratively corrected Chromosome XII heatmap from *cdc15*
1014 cells arrested in anaphase. Yellow arrow indicates the interaction between CEN12 and the
1015 rDNA-adjacent bin. **(D)** Contact map showing interactions between centromeres in the anaphase-
1016 arrested *cdc15* mutant. **(E)** Model for cohesin and Sir2 depletion from the rDNA of aged mother
1017 cells. Cohesin is initially retained at centromeres (Middle Age, black arrow), and then ultimately
1018 lost in the oldest cells. ERCs begin to form during middle age and may contribute in a self-
1019 perpetuating cycle resulting in chronic destabilization of the rDNA array due to loss of cohesin,
1020 RENT, and the cohibin complex (red).

Figure 1

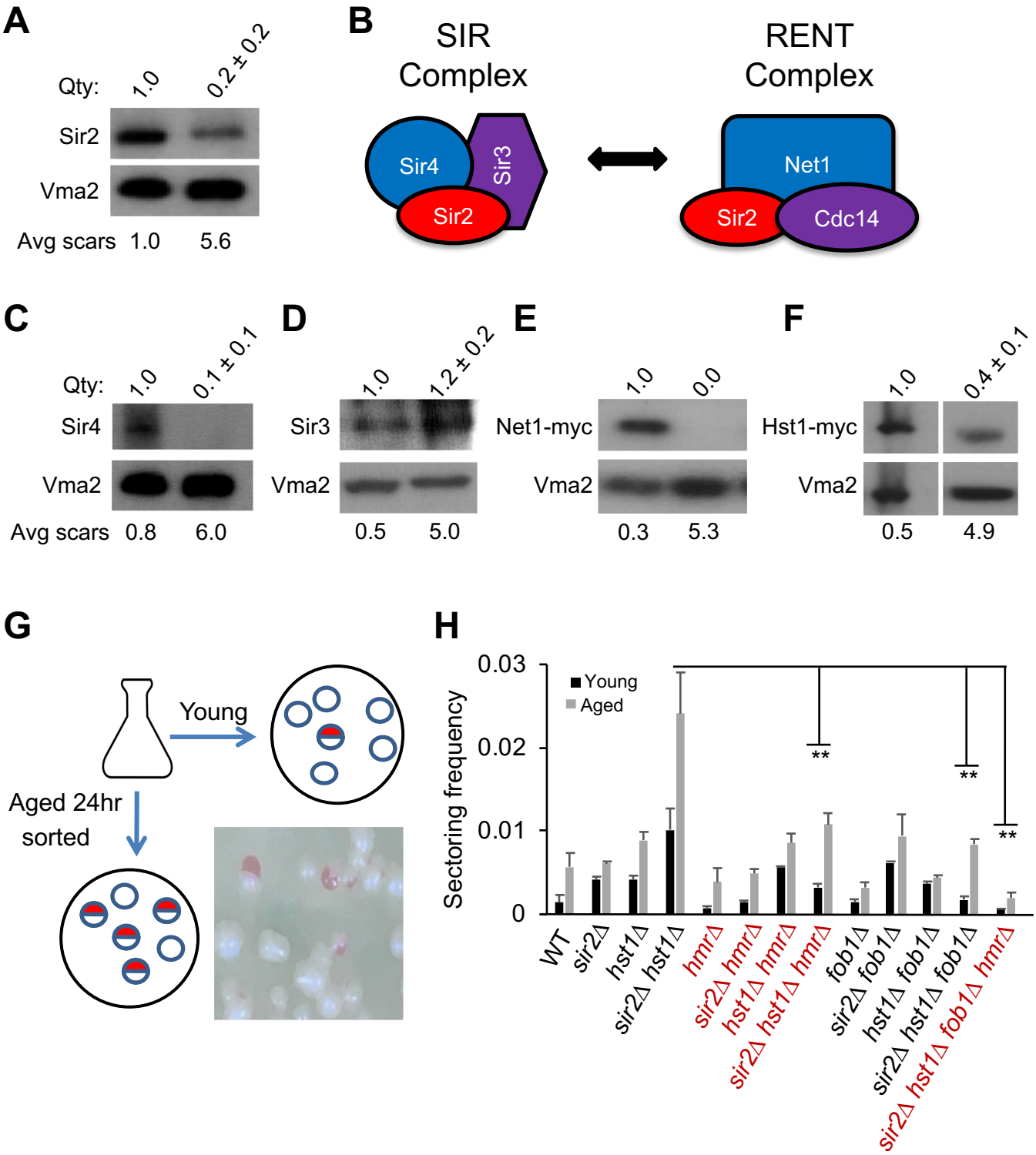
A
Qty:
1.0
0.2 ± 0.2
Sir2
Vma2
Avg scars 1.0 5.6
B
SIR Complex
Sir4
Sir3
Sir2
RENT Complex
Net1
Sir2
Cdc14
C
Qty:
1.0
0.1 ± 0.1
Sir4
Vma2
Avg scars 0.8 6.0
D
1.0
1.2 ± 0.2
Sir3
Vma2
0.5 5.0
E
1.0
0.0
Net1-myc
Vma2
0.3 5.3
F
1.0
0.4 ± 0.1
Hst1-myc
Vma2
0.5 4.9
G
Young
Aged 24hr sorted
H
Sectoring frequency
0.03
0.02
0.01
0
Young
Aged
**
**
**
WT
sir2Δ
hst1Δ
sir2Δ hst1Δ
hmrΔ
sir2Δ hmrΔ
hst1Δ hmrΔ
sir2Δ hst1Δ hmrΔ
fob1Δ
sir2Δ fob1Δ
hst1Δ fob1Δ
sir2Δ hst1Δ fob1Δ
sir2Δ hst1Δ fob1Δ hmrΔ

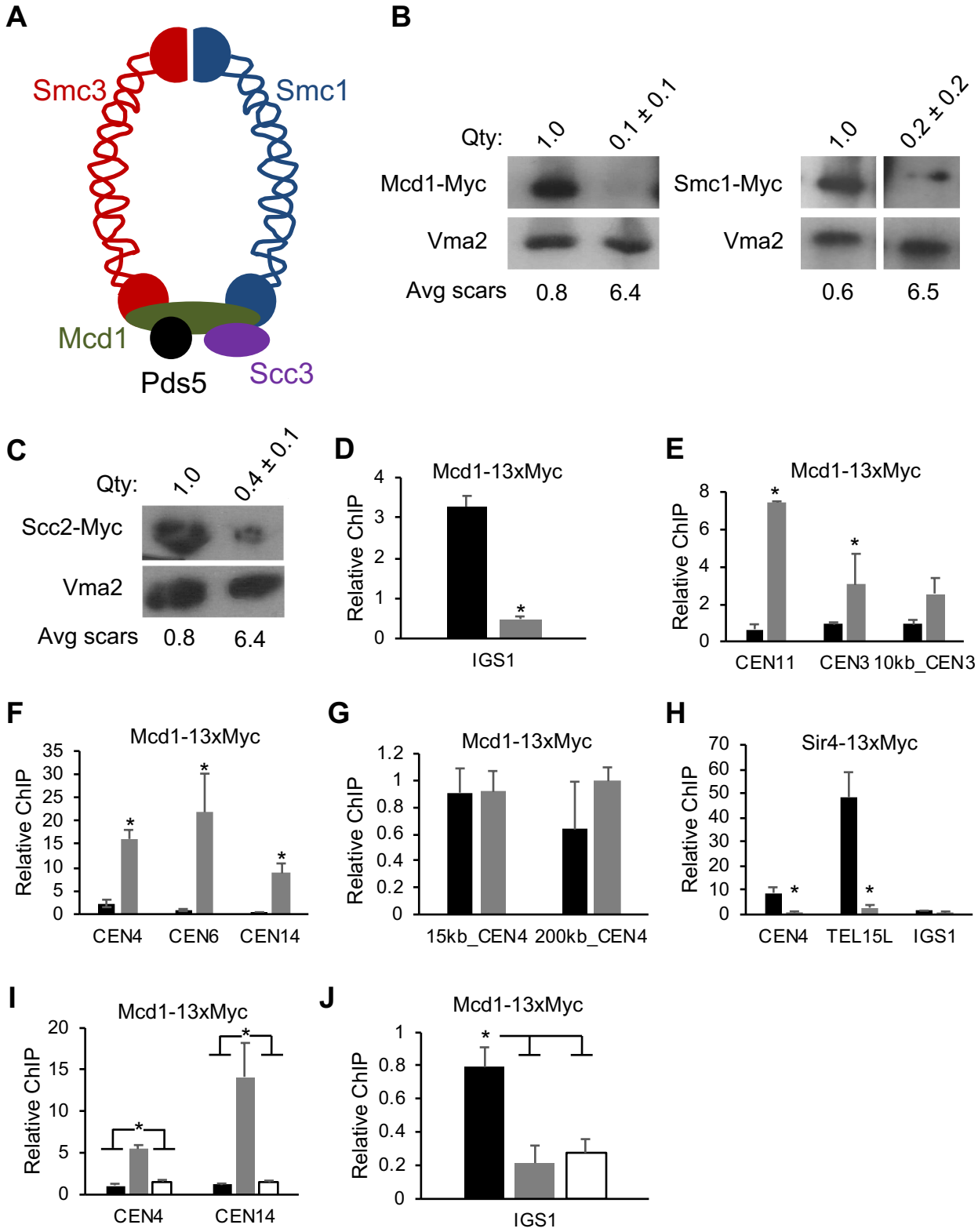
A
Smc3
Smc1
Mcd1
Pds5
Scc3
B
Qty:
1.0
0.1 ± 0.1
Mcd1-Myc
Vma2
Avg scars
0.8
6.4
1.0
0.2 ± 0.2
Smc1-Myc
Vma2
0.6
6.5
C
Qty:
1.0
0.4 ± 0.1
Scc2-Myc
Vma2
Avg scars
0.8
6.4
D
Mcd1-13xMyc
Relative ChIP
IGS1
E
Mcd1-13xMyc
Relative ChIP
CEN11
CEN3
10kb_CEN3
F
Mcd1-13xMyc
Relative ChIP
CEN4
CEN6
CEN14
G
Mcd1-13xMyc
Relative ChIP
15kb_CEN4
200kb_CEN4
H
Sir4-13xMyc
Relative ChIP
CEN4
TEL15L
IGS1
I
Mcd1-13xMyc
Relative ChIP
CEN4
CEN14
J
Mcd1-13xMyc
Relative ChIP
IGS1

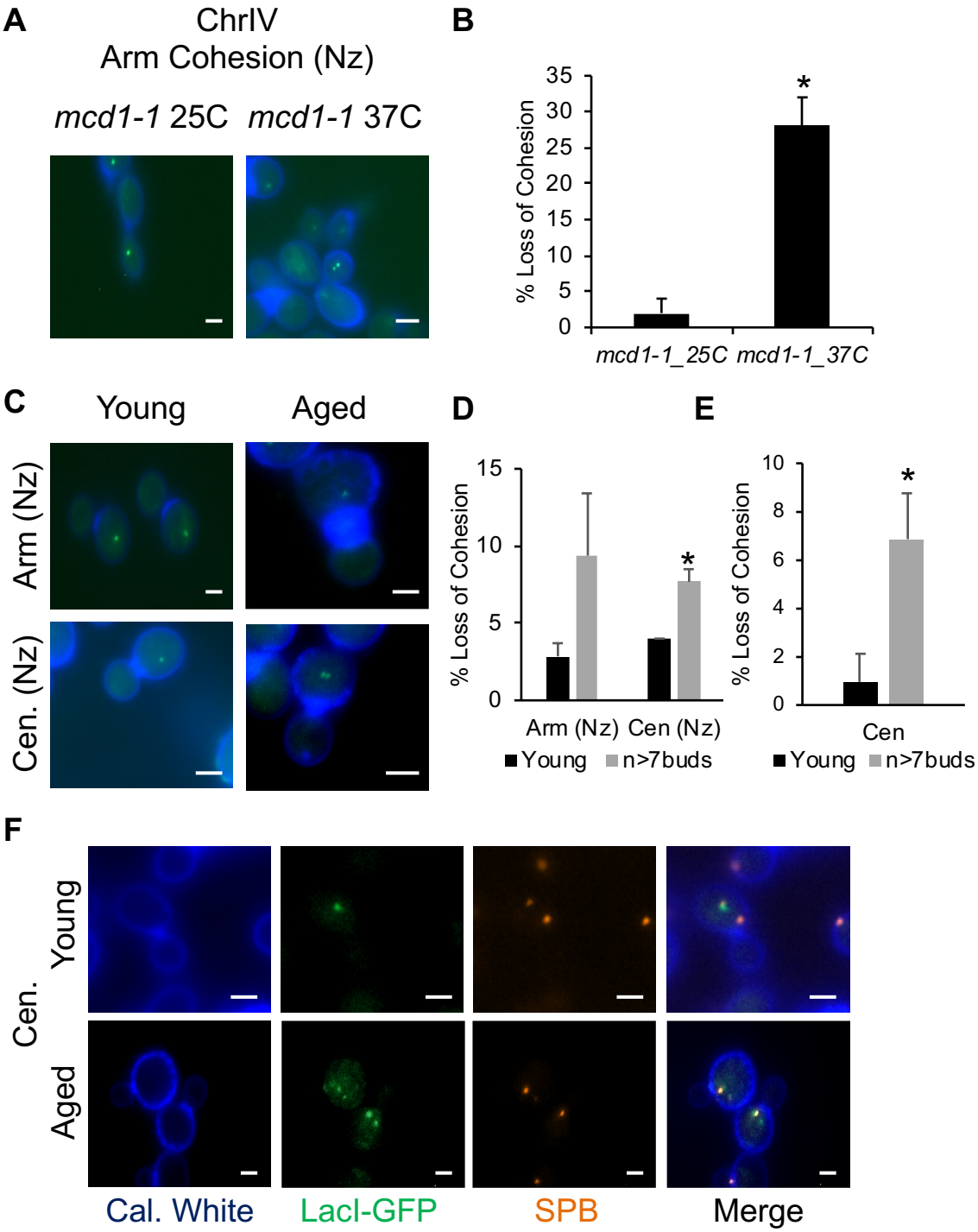
A
ChrIV
Arm Cohesion (Nz)
mcd1-1 25C
mcd1-1 37C
B
% Loss of Cohesion
35
30
25
20
15
10
5
0
*
mcd1-1_25C
mcd1-1_37C
C
Young
Aged
Arm (Nz)
Cen. (Nz)
D
% Loss of Cohesion
15
10
5
0
*
Arm (Nz)
Cen (Nz)
Young
n>7buds
E
% Loss of Cohesion
10
8
6
4
2
0
*
Cen
Young
n>7buds
F
Cen.
Young
Aged
Cal. White
LacI-GFP
SPB
Merge

Figure 4

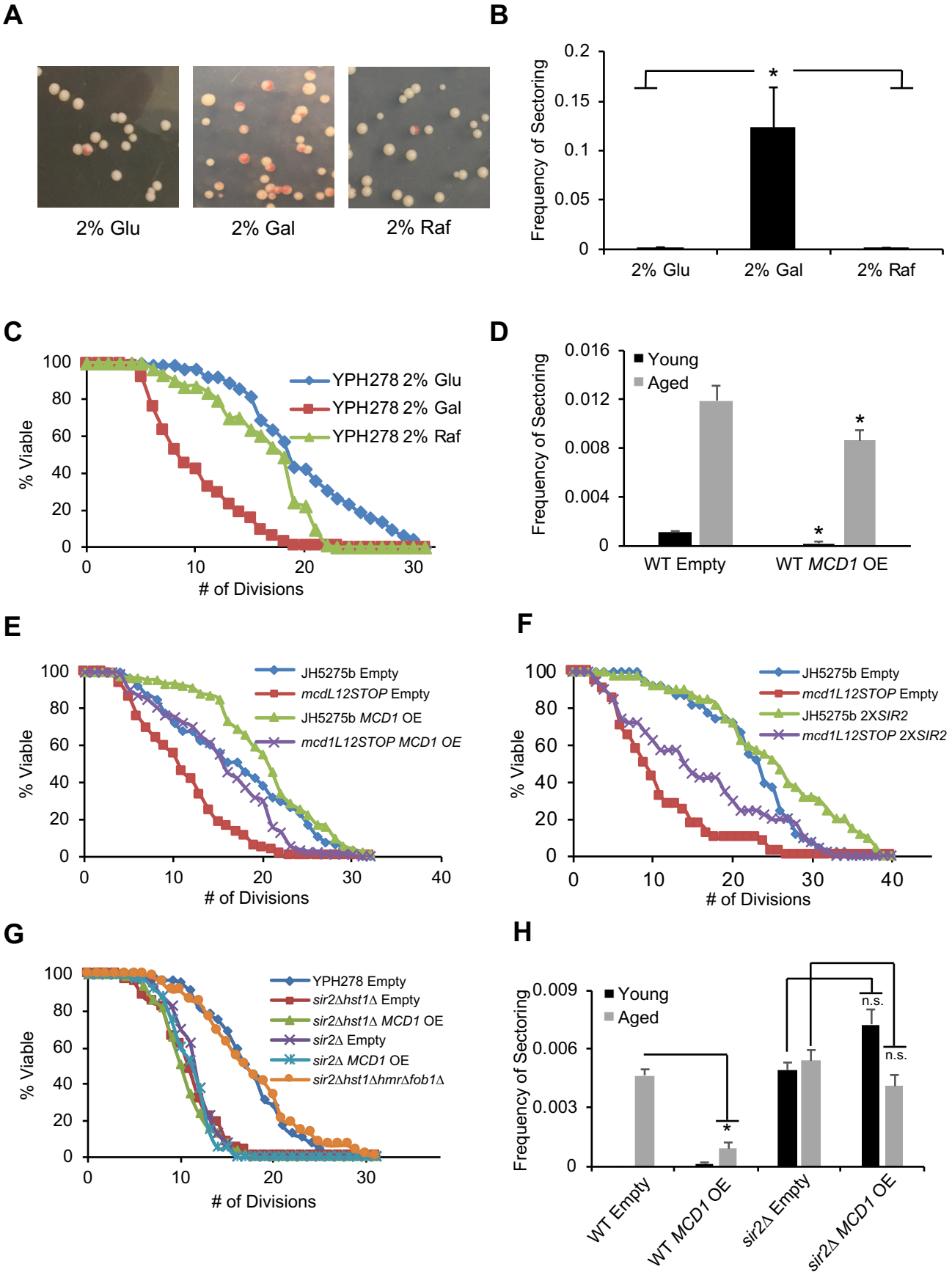
A
2% Glu
2% Gal
2% Raf
B
Frequency of Sectoring
0.2
0.15
0.1
0.05
0
*
2% Glu
2% Gal
2% Raf
C
% Viable
100
80
60
40
20
0
YPH278 2% Glu
YPH278 2% Gal
YPH278 2% Raf
0
10
20
30
# of Divisions
D
Frequency of Sectoring
0.016
0.012
0.008
0.004
0
Young
Aged
*
*
WT Empty
WT MCD1 OE
E
% Viable
JH5275b Empty
mcdL12STOP Empty
JH5275b MCD1 OE
mcd1L12STOP MCD1 OE
0
10
20
30
40
# of Divisions
F
% Viable
JH5275b Empty
mcd1L12STOP Empty
JH5275b 2XSIR2
mcd1L12STOP 2XSIR2
0
10
20
30
40
# of Divisions
G
% Viable
YPH278 Empty
sir2Δhst1Δ Empty
sir2Δhst1Δ MCD1 OE
sir2Δ Empty
sir2Δ MCD1 OE
sir2Δhst1Δhmr1Δfob1Δ
0
10
20
30
# of Divisions
H
Frequency of Sectoring
0.009
0.006
0.003
0
Young
Aged
*
n.s.
n.s.
WT Empty
WT MCD1 OE
sir2Δ Empty
sir2Δ MCD1 OE

Figure 5

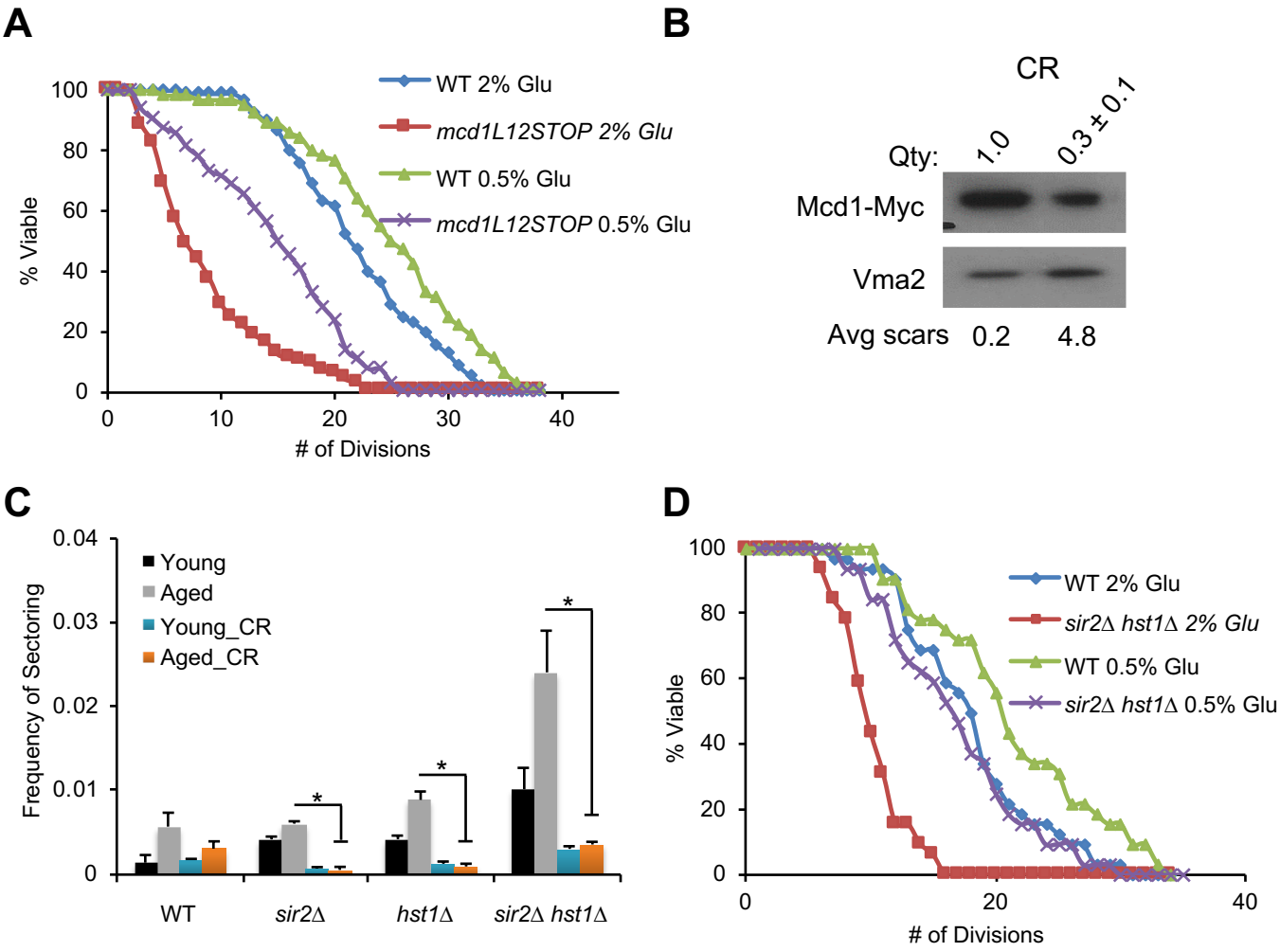
A
100
80
60
40
20
0
% Viable
0
10
20
30
40
# of Divisions
WT 2% Glu
mcd1L12STOP 2% Glu
WT 0.5% Glu
mcd1L12STOP 0.5% Glu
B
CR
Qty:
1.0
0.3 ± 0.1
Mcd1-Myc
Vma2
Avg scars
0.2
4.8
C
0.04
0.03
0.02
0.01
0
Frequency of Sectoring
Young
Aged
Young_CR
Aged_CR
*
*
*
WT
sir2Δ
hst1Δ
sir2Δ hst1Δ
D
100
80
60
40
20
0
% Viable
0
20
40
# of Divisions
WT 2% Glu
sir2Δ hst1Δ 2% Glu
WT 0.5% Glu
sir2Δ hst1Δ 0.5% Glu

Figure 6

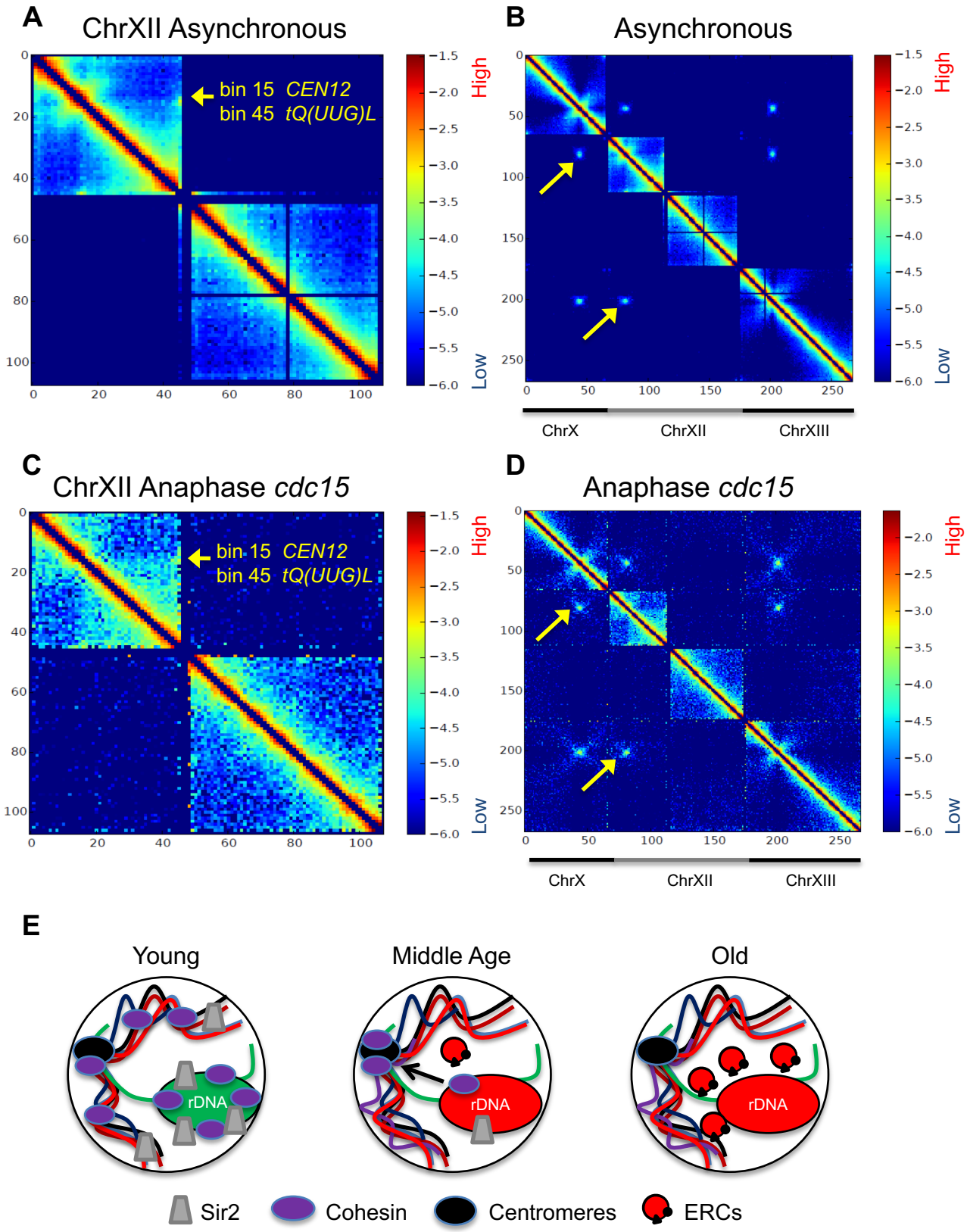
A
ChrXII Asynchronous
bin 15 CEN12
bin 45 tQ(UUG)L
High
Low
B
Asynchronous
ChrX
ChrXII
ChrXIII
C
ChrXII Anaphase cdc15
bin 15 CEN12
bin 45 tQ(UUG)L
D
Anaphase cdc15
E
Young
Middle Age
Old
rDNA
Sir2
Cohesin
Centromeres
ERCs